NCC 2-55
AMES GRANT
IN-09-CR
222706
P-36

JOINT INSTITUTE FOR AERONAUTICS AND ACOUSTICS

National Aeronautics and
Space Administration

Ames Research Center

Stanford University

JIAA TR - 89

DESIGN AND CALIBRATION OF THE MIXING LAYER AND WIND TUNNEL

BY

James H. Bell and Rabindra D. Mehta

Stanford University
Department of Aeronautics and Astronautics
Stanford, CA 94305

MAY 1989

(NASA-CR-185472) DESIGN AND CALIBRATION OF THE MIXING LAYER AND WIND TUNNEL (Stanford Univ.) 36 p CSCL 01E

N89-26866

Unclas
G3/09 0222706

ABSTRACT

This report contains a detailed account of the design, assembly and calibration of a wind tunnel specifically designed for free-shear layer research. The construction of this new facility was motivated by a strong interest in the study of plane mixing layers with varying initial and operating conditions. The *Mixing Layer Wind Tunnel* is located in the Fluid Mechanics Laboratory at NASA Ames Research Center. The tunnel consists of two separate legs which are driven independently by centrifugal blowers connected to variable speed motors. The blower/motor combinations are sized such that one is smaller than the other, giving maximum flow speeds of about 20 and 40 m/s, respectively. The blower speeds can either be set manually or via the Microvax II computer. The two streams are allowed to merge in the test section at the sharp trailing edge of a slowly tapering splitter plate. The test section is 36 cm in the cross-stream direction, 91 cm in the spanwise direction and 366 cm in length. One test section side-wall is slotted for probe access and adjustable so that the streamwise pressure gradient may be controlled. The wind tunnel is also equipped with a computer controlled, three-dimensional traversing system which is used to investigate the flow fields with pressure and hot-wire instrumentation. The wind tunnel calibration results show that the mean flow in the test section is uniform to within $\pm 0.25\%$ and the flow angularity is less than $0.25°$. The total streamwise free-stream turbulence intensity level is approximately 0.15%. Currently the wind tunnel is being used in experiments designed to study the three-dimensional structure of plane mixing layers and wakes.

NOMENCLATURE

AR:	Test section aspect ratio
c:	Contraction ratio
CFM:	Volume flow rate in cubic feet per minute
C_f:	Skin friction coefficient
C_p:	Pressure coefficient on contraction wall
d:	Screen wire diameter
D:	Honeycomb cell diameter
H:	Boundary layer shape factor
HP:	Motor horse power
H_e:	Contraction height at exit
H_i:	Contraction height at inlet
K:	Screen pressure drop coefficient
L:	Contraction length *or* honeycomb cell length
l:	Screen mesh length
p:	Static pressure
Δp:	Static pressure drop or rise across element
P:	Total pressure
q:	Dynamic pressure
RPM:	Blower revolutions per minute
Re_L:	Reynolds number, UL/ν
U, V, W:	Mean velocity in the X,Y,Z directions, respectively
U_e:	Free-stream velocity in the wind tunnel test section
u', v', w':	Fluctuating velocity components in the X,Y,Z directions, respectively
u, v, w:	Instantaneous velocity in the X,Y,Z directions, respectively, e.g. u = U + u'
X, Y, Z:	Cartesian coordinates for streamwise, normal, and spanwise directions, respectively
β:	Screen open-area ratio
δ_{99}:	Boundary layer thickness
θ:	Boundary layer momentum thickness
ν:	Kinematic viscosity
ρ:	Density
$\bar{\ }$:	(overbar) Time-averaged quantity
$(\ )_{max}$:	Maximum value at station

1. INTRODUCTION

Wind tunnels of various forms and designs have been widely used for model tests and basic fluid flow research since about the turn of the century. Since the 1930s, when the strong effect of free-stream turbulence on shear layers became apparent, emphasis has been laid on wind tunnels with low levels of turbulence and unsteadiness (Prandtl, 1933). A wind tunnel is still an essential tool in engineering, even with today's improved computing capabilities. Wind tunnel design always has been, and will be, a combination of art, science and commonsense. Traditionally, it has been difficult and unwise to make firm design rules for all the components of a wind tunnel, mainly due to the wide variety of tunnel designs and the lack of understanding of the flow, especially the turbulent boundary layers encountered in many of the tunnel components. Therefore, a more feasible and sensible approach was followed whereby approximate design boundaries were predicted based on exisiting "successful" designs. Such design guidelines for low-speed wind tunnels were first given by Bradshaw and Pankhurst (1964).

In the late 1970s, a project was initiated by one of the present authors, designed to gain a better understanding of the performance of "blower" tunnel components (Mehta, 1978). A blower tunnel is defined as an open-circuit wind tunnel driven by a centrifugal blower at the entry. The main aim of the study was to make the design of these components more scientific, logical and hence successful.

Design rules for wide-angle diffusers were derived, based mainly on correlations of data collected from existing designs (Mehta, 1977). A wide-angle diffuser is defined as one which expands so rapidly that separation can only be avoided by some form of boundary layer control. Screens are by far the most popular means of preventing separation in wide-angle diffusers. This is in addition to the more accepted role of screens in improving the flow uniformity and reducing the turbulence intensity levels (Dryden and Schubauer, 1947). A detailed experimental investigation was carried out on the effects of different types of screens (metal and plastic) on turbulent flow, in particular turbulent boundary layers (Mehta, 1984 and 1985). The boundary layer turbulence was found to be reorganized and the thickness reduced, thus making the layer less susceptible to separation. The effects of screen inclination on pressure drop coefficient and deflection coefficient were also established. Tests on single-inlet centrifugal blowers revealed that the outlet flow was in the form of a large longitudinal swirl which may be used to advantage in preventing separation on the wide-angle diffuser walls (Mehta, 1977). Design guidelines based on the results of this research project were given in Mehta and Bradshaw (1979).

In wind tunnels designed for shear layer research, the two-dimensionality of the flow (or the lack of it) is also of considerable concern (Morkovin, 1979). In a separate experimental study, the effect of screens, honeycombs and centrifugal blowers on the two-dimensionality of a boundary layer on the test section floor was investigated (Mehta and Hoffmann, 1986 and 1987). Surveys of the spanwise variation in surface shear stress in three blower tunnels revealed that the main component responsible for altering the spanwise properties of the test section boundary layer was the last screen, thus confirming previous findings (e.g. Bradshaw, 1965). It was further confirmed that a screen with varying open-area ratio (due to dirt accretion, for example), produced an unstable flow. However, contrary to

popular belief, it was also found that for given incoming conditions and a screen free of imperfections, the screen open-area ratio *alone* was not enough to describe its performance.

More recently, an iterative design procedure was developed for two- or three-dimensional contractions installed on small, low-speed wind tunnels (Bell and Mehta, 1988, 1989a). The procedure consisted of first computing the potential flow field, and hence the pressure distributions, along the walls of a contraction of given size and shape using a three-dimensional numerical panel method. The pressure (or velocity) distributions were then fed into two-dimensional boundary layer codes to predict the behavior of the boundary layers along the walls. For small, low-speed contractions it was shown that the boundary layer behavior could be adequately predicted by assuming that a laminar boundary layer originated from stagnation conditions at the contraction entry and remained laminar throughout passage through the "successful" contraction designs.

The design of the new wind tunnel was based on the results and analyses of all these investigations. The unique aspect of the tunnel is its ability to easily generate mixing layers with varying initial and operating conditions. Turbulent mixing layers play many important roles in practical aerodynamics. Mixing layers govern the rate of mixing in combustion chambers and flow reactors, for example, and are also responsible for most of the broadband noise generated in propulsion systems. Furthermore, the flow over modern aircraft wings with multiple airfoils is dominated by complex interactions involving free-shear flows, including mixing layers. The ability to control the structure and development, and hence mixing capabilities, of this shear flow would therefore have a vital impact on many engineering applications.

Section 2 of this report contains a detailed description of the individual components of the wind tunnel. The wind tunnel performance characteristics are presented in Section 3 while the flow quality measurements are given and discussed in Section 4. Some concluding remarks, including a brief description of ongoing research work in the new facility, are given in Section 5.

2. DESCRIPTION OF THE WIND TUNNEL COMPONENTS

The overall schematic of the Mixing Layer Wind Tunnel is shown in Fig. 1. Air is drawn-in by two separate blowers, one larger than the other, and passed through separate diffusers, flow conditioning elements and two separate but identical contraction sections into the test section. The selection or design of the individual components is now discussed starting from the upstream (intake) end.

2.1 Drive Systems

Over the past couple of decades, centrifugal blowers with backward-facing "airfoil-type" impellers have emerged as the optimum choice for driving open-circuit wind tunnels. Centrifugal blowers run with reasonable steadiness and efficiency over a wide range of flow conditions with varying tunnel power factor (defined as the ratio of shaft input power to tunnel output power) because the whole blade span operates at nominally the same lift

coefficient. The noise and pulsations generated by a centrifugal blower are generally found to be adequately low, even at off-design conditions. In blowers with single inlets, such as those used on the present tunnel, the impeller is asymmetrically positioned so as to accommodate the entry bellmouth within the blower casing. This asymmetry produces a swirling flow at the blower outlet which is found to be independent of the advance ratio; it is dependent on the ratio of rotor to casing width. The vortex-type outlet flow can be used to advantage to maintain wall flow attachment in the wide-angle diffuser. This compensates for the non-uniformity of the flow which is later improved by the screens in the wide-angle diffuser and the settling chamber.

The "low-speed" leg of the present wind tunnel is driven by a size 223 Acoustafoil blower (New York Blower Company) — a 5,000 CFM centrifugal blower with a 56 cm impeller consisting of backward-facing, airfoil-type blades. The outlet dimensions of this blower are 43×64 cm and it is powered by a 5 HP electric motor (Eaton Corporation, Dynamatic Ajusto Spede, Model AC-186). The motor speed, and thus the flow rate, is set using an Eaton Dynamic Model 4000 Ajusto Spede motor contoller. A feedback circuit controlling the eddy-current clutch maintains the motor at a constant speed; mean flow velocity through the test section varies by less than 1% over the time of a typical run lasting about two hours. This blower/motor combination was retrived from the now discarded Shear Layer Wind Tunnel. Aside from considerations of cost, it was felt that the smaller blower would show better stability at low tunnel speeds, and so it would be advantageous to have a dedicated low-speed side.

The high-speed side blower is a size 339 SWSI Class II Acoustafoil Centrifugal Fan (New York Blower Company). This blower delivers 15,000 CFM with a 86 cm impeller also consisting of backward-facing, airfoil-type blades. The blower has outlet dimensions of 61×94 cm and is powered by a 20 HP electric motor (Eaton Corporation, Dynamatic Ajusto Spede Model ACM-280). As with the smaller motor, speed control is achieved by adjusting the eddy-current clutch through a feedback circuit. The flow rate of both blowers can be controlled either manually or through a D/A output signal from a Microvax II computer. The motors are physically isolated from the blowers so as to reduce vibration as much as possible, and the only physical connection between the blowers and the rest of the wind tunnel are duct tape couplings sealing the blower/diffuser junctions. The contributions to free-stream turbulence due to motor/blower vibration, blade passing frequency, and irregularities in the blower have been measured and found to be acceptably small, as discussed below in Section 4.3.

A $122 \times 122 \times 122$ cm filter box covers the inlet of the high-speed side blower, and a $91 \times 91 \times 91$ cm filter box covers the intake section of the low-speed side blower. The filter material consists of two layers of cheesecloth which has been found to effectively remove most of the dust in the incoming air while imposing only a negligible pressure drop; with the current set of flow-conditioning elements, the small and large blowers can generate flow speeds in the test section of up to 20 m/s and 40 m/s, respectively. The filters are considered to be effective since hot-wire drift, attributable to dirt accretion, has been found to be negligibly small.

2.2 Wide-Angle Diffusers

Although diffusers form an itegral part of almost all wind tunnels, their flow characteristics have still to be fully understood. The flow through a diffuser inevitably depends on its geometry, defined by the area ratio, wall expansion angle, cross-sectional shape and wall contour. Other parameters such as geometric and flow conditions at entry and exit also affect the diffuser performance. With an arbitrary combination of these parameters, the flow through a diffuser becomes extremely difficult to predict in detail. The issue is further complicated by the occasional presence of boundary layer separation caused by the adverse pressure gradients necessarily present in a diffuser. It was in fact a separation in a conical diffuser that inspired Prandtl to come up with the boundary layer concept in 1904. A "wide-angle" diffuser is defined as a diffuser in which the cross-sectional area increases so rapidly that separation can be avoided only by using boundary layer control. A wide-angle diffuser is used to reduce the length needed for a given area ratio rather than effecting a pressure recovery, and in blower tunnels such as the present one, it is installed between the blower and settling chamber.

Screens are the most popular means of boundary layer control in diffusers. A screen, besides removing the direct effects of boundary layer growth and incipient separation, effectively gives the layer "a new lease of life" — the boundary layer thickness is reduced and the existing turbulence almost completely obliterated, thus forming a "new" boundary layer (Mehta, 1984 and 1985). In addition, screens also help to improve the flow nonuniformity and reduce the flow angularity — this is particularly useful for straightening the swirling type flow produced by a single-inlet centrifugal blower. For a diffuser using screens for boundary layer control, the important parameters are found to be the diffuser angle, area ratio, number of screens and the overall pressure drop coefficient of the screens. Mehta (1977 and 1978) collected data from over a hundred wide-angle diffuser designs (successful and unsuccessful) and plotted charts for relevant parameters from which design rules were derived. The number of screens required within the diffuser is determined from the diffuser angle and the area ratio. The area ratio also gives the overall required pressure drop coefficient from the screens in order to avoid separation.

The present rectangular wide-angle diffuser designs were broadly based on these derived rules. The small diffuser expands from 43×64 cm to 91×137 cm over a length of 2.9 m, giving a maximum included angle of 18.2° and an area ratio of 4.75. The larger diffuser expands from 61×94 cm to 91×137 cm over a length of 2.4 m, giving an included angle of 17.6° and an area ratio of 2.25. Each diffuser contains two relatively coarse screens with $\beta = 64.6\%$ (14 mesh, $d = 0.36$ mm), one at the upstream end and one at the downstream junction (Fig. 2). At the upstream end, the screen is "sandwiched" between the diffuser flange and a 15 cm long coupling flange, while the downstream screen is sandwiched between the diffuser and settling section flanges. In order to properly seal the junctions where a screen was sandwiched, the flange surface was lined with a rubber compound.

2.3 Settling Chamber (Flow Conditioning Section)

In open-circuit blower tunnels, settling chambers are created rather than designed since the frames containing the flow conditioning elements, clamped together, generally

form the settling chamber. The flow conditioning elements usually consist of a honeycomb and screens, the number and overall pressure drop depending on the turbulence level requirements in the test section. The settling chamber on the mixing layer wind tunnel consists of a 30.5 cm long "settling length" and a 44.5 cm stack of seven frames, each 6.4 cm wide. Each side of the settling chamber (high-speed and low-speed) consists of a honeycomb and five screens, as illustrated in Fig. 2.

The most efficient device for removing swirl and lateral mean velocity variations in the flow is a honeycomb, as long as the flow yaw angles are not greater than about 10°. Large yaw angles cause the honeycomb cells to "stall" which reduces their effectiveness besides increasing the pressure loss and causing flow nonuniformity. If severe yaw or swirl is expected in the incoming flow, it is advisable to install screens upstream of the honeycomb, so that the flow angles are reduced. A screen with $K = 1.5$ reduces yaw and swirl angles by a factor of 0.7 for swirl angles of about 40°, so multiple screens would be required upstream of the honeycomb in this case. The honeycomb should also be installed some distance downstream of the wide-angle diffuser exit, so that the flow static pressures and angles have had a chance to become more uniform. For this very reason, in the present wind tunnel, the diffuser sections are followed by 30.5 cm long, constant area "settling sections" (Fig. 2). Also, the honeycomb on each side is preceded by a screen with $\beta = 62.4\%$ (28 mesh, $d = 0.19$ mm).

An incidental effect of honeycombs is to reduce the turbulence level in the flow. Essentially, the lateral components of turbulence, like those of mean velocity, are inhibited by the honeycomb cells and almost complete annihilation is achieved in a length equivalent to about 5-10 cell diameters. Honeycombs themselves shed small-scale turbulence, the level of which is found to be higher when the cell flow is laminar than when it is turbulent: this is attributed to a basic instability of the laminar near wakes which leads to transition, and hence high turbulence intensities, in the free-shear layer (Mehta, 1978, Bell and Mehta, 1989b). Note that the cell flow in most small, low-speed wind tunnel honeycombs is laminar. Now since the shear layer instability in the near wake has a strength proportional to the shear layer thickness, the *net* reduction (ratio of turbulence suppressed to that generated) is greatest for the shortest honeycomb.

For maximum overall benefit, the optimum cell length has been found to be about 6-8 times its diameter. As for cell size, in general, approximately 150 cells per settling chamber "diameter" or 25,000 cells total are found to be adequate. Ideally, the cell size should be smaller than the smallest lateral wavelength of the velocity variation. This implies that the choice of cell size should also depend somewhat on the size of the blower generating the flow, since this determines the initial (input) flow scales and also on other elements such as screens which may be installed in the wide-angle diffuser. The selection of the two aluminum honeycombs for the present wind tunnel were based on all these criteria. The high-speed side honeycomb is 5.1 cm long with 6.4 mm cells ($L/D = 8$) while the low-speed side honeycomb is somewhat smaller with 3.2 mm cells over a 2.5 cm length ($L/D = 8$). The cross-sectional shape of the cells is not critical and it is usually determined by availabilty; the cell shape on both the present honeycombs is hexagonal.

Screens have been used to improve flow quality in wind tunnels since the 1930s. Prandtl (1933) noted that the velocity distribution improved when screens were installed in

a wind tunnel and he gave a simple theory for this effect. The action of screens in reducing the turbulence intensity levels became apparent later. Dryden and Schubauer (1947) gave a physical explanation for this effect: turbulent eddies of larger scale than the screen mesh size are decreased, and although at the same time smaller scale eddies may be introduced, they decay much more rapidly than the original large-scale motions would in the absence of the screen. The expected overall effect is that at some distance downstream, both the turbulence intensity and scale have been reduced.

Screens are normally made of metal wires interwoven to form square or rectangular meshes, and are usually installed in the settling chamber to improve the mean flow uniformity and to reduce the intensity of the oncoming turbulence. A screen also refracts the incident flow towards the local normal. The action of a screen is described in terms of two parameters, namely the pressure drop coefficient and the deflection coefficient. The factors of reduction of mean velocity variation and turbulence intensity by screens are tabulated in Mehta (1977). Screens make the flow uniform by imposing a static pressure drop proportional to velocity squared. A screen with a pressure drop coefficient of about two removes nearly all variation in the longitudinal mean velocity. Dryden and Schubauer (1947) showed that, for a given pressure drop, a greater reduction in turbulence intensity is obtained by using multiple screens, each with a comparatively low pressure drop coefficient. The most optimum formulation for the screen pressure drop coefficient (see Mehta, 1978) is that due to Wieghardt (1953) and is defined as:

$$K = \frac{\Delta p}{\frac{1}{2}\rho U^2} = 6.5\frac{(1-\beta)}{\beta^2}\left[\frac{Ud}{\beta\nu}\right]^{-1/3} \tag{1}$$

In the present wind tunnel design, the four screens downstream of the honeycomb are identical on both sides of the settling chamber (Fig. 2). The first screen is 28 mesh, with 0.19 mm wire diameter and $\beta = 62.4\%$. The next two screens are 42 mesh, with 0.14 mm wire diameter and $\beta = 59.1\%$. The last screen is 44 mesh, with 0.14 mm wire diameter and $\beta = 57.5\%$. The order of the screens is chosen such that the mesh size decreases with downstream position. This was done in an attempt to gradually decrease the scale of the oncoming turbulence since some recent results (Mehta, 1978) have further confirmed the belief that the scale of the turbulence is reduced by a screen. All the screens have an open area ratio of greater than 57% since low β screens have been known to produce instabilities resulting from a random coalition of jets and wakes amalgamating to form weak longitudinal vortices (Mehta and Hoffmann, 1986 and 1987).

There are two important considerations when choosing the optimum spacing between the flow conditioning elements. For the pressure drops through the screens to be completely independent of each other, the spacing should be such that the static pressure has fully recovered from the perturbation before reaching the next screen. For full benefits from the turbulence-reduction point of view, the minimum spacing should perhaps be of the order of the large energy containing eddies. The basic design philosophy is that the screens must be placed sufficiently far apart so that they act as individual elements for which the behavior

is well understood. It has been found (empirically) that a spacing equivalent to 5% of the settling chamber diameter performs successfully, and was hence used in the present design.

The last frames in the settling chamber do not contain any flow conditioning elements — they were left empty for two main reasons. Firstly, they allowed the flow to recover from the effects of the last screen before feeling the effects due to the contraction entry. Secondly, they enabled a smooth transition from the frame surface to the splitter plate; the splitter plate was designed to slide onto indentations machined on the last pair of frames.

2.4 Contraction Section

Contraction sections form an integral part of all wind tunnels, whether designed for basic fluid flow research or model testing. They are normally installed upstream of the test section and serve two main purposes. Firstly, since the total pressure remains constant through the contraction, both mean and fluctuating velocity variations are reduced to a smaller fraction of the average velocity at a given cross-section. Secondly, a contraction increases the flow mean velocity and this allows the flow conditioning elements to be placed in a lower speed region, thus reducing the pressure losses through these components. The most important single parameter in determining these effects is the contraction ratio, c. The factors of reduction of mean velocity variation and turbulence intensity for axisymmetric contractions were derived theoretically by Batchelor (1953) using the rapid distortion theory and are given as:

(i) u-component mean velocity, U: $1/c$
(ii) v or w-component mean velocity, V or W: $\sqrt{c}$
(iii) u-component r.m.s. intensity, u': $\frac{1}{2c}[3(ln4c^3 - 1)]^{1/2}$
(iv) v or w-component r.m.s. intensity, v' or w': $\frac{(3c)^{1/2}}{2}$

A contraction is less efficient in suppressing longitudinal turbulence than mean velocity variation. In absolute level, the lateral turbulence intensities (v' and w') are enhanced while the streamwise intensity (u') is reduced. The reduction of fractional variation of the lateral component is therefore much less than that of the streamwise component, so it should be the desired reduction in the former (together with the desired mean flow uniformity) which decides the contraction ratio. Contraction ratios of between 6 and 10 are found to be adequate for most small, low-speed wind tunnels — defined as tunnels with a test section cross-sectional area of less than about 0.5 m^2 and free-stream velocities of less than about 40 m/s.

Another contraction parameter that has to be selected, a priori, is the cross-sectional shape. In order to avoid crossflows and boundary layer separation in the corners, the ideal cross-sectional shape is circular. However, in the absence of separation, the secondary flows in the corners tend to remain localized, without any significant effect on the test section flow quality (Mehta, 1978). The cross-sectional shape for modern day contractions is, therefore, almost always chosen to match the other tunnel components which are normally square or rectangular.

The wall shape design of a contraction of given area ratio and cross-section centers

on the production of a uniform and steady stream at its outlet. These conditions can be generally met by making the contraction section very long so that the length is equivalent to several times the inlet height. However, another desirable flow quality is minimum boundary layer thickness (in a laminar state) at the contraction exit. This suggests that the contraction length should be minimized so that the boundary layer growth is also minimized. Shorter contractions are also, of course, desirable for saving in cost and space. However, the risk of boundary layer separation increases as the contraction length is reduced. The danger of boundary layer separation results from the presence of regions of adverse pressure gradient on the walls at each end of a contraction of finite length. The adverse pressure gradients become stronger as the contraction length is decreased. In general, the boundary layer is less liable to separate at the contraction exit, due to its increased skin friction coefficient caused by passage through the strong favorable pressure gradient. Also, the concave curvature at the contraction inlet has a destabilizing effect on the boundary layer, in contrast to the convex curvature near the exit which has a stabilizing effect (Bradshaw, 1973). In addition to unnecessary thickening of the boundary layer, separation also generally leads to flow unsteadiness, which cannot be easily eliminated from the test-section flow. A design satisfying all criteria will be such that separation is just avoided (implying a minimum acceptable length) and the exit non-uniformity is equal to the maximum tolerable level for a given application (typically less than 1% variation in mean streamwise velocity outside the boundary layers). Since a satisfactory direct design method for the contraction wall shape was not readily available, a new design strategy was pursued.

An iterative design procedure was developed for the contraction to be installed on the present mixing layer wind tunnel (Bell and Mehta, 1988 and 1989a). The procedure consisted of first computing the potential flow field and hence the pressure distributions along the walls of a contraction of given size and shape using a three-dimensional numerical panel method. The wall pressure or velocity distributions were then fed into two-dimensional boundary layer codes to predict the behavior of the boundary layers along the walls. For small, low-speed contractions it was shown that the assumption of a laminar boundary layer originating from stagnation conditions at the contraction entry and remaining laminar throughout passage through the "successful" designs was justified. This hypothesis was confirmed by comparing the predicted boundary layer data at the contraction exit with measured data in existing wind tunnels. The measured boundary layer momentum thicknesses at the exit of three existing contractions, two of which were 3-D, were found to lie within 10% of the predicted values, with the predicted values generally lower.

Once the computational procedure had been validated, it was used to select the optimum wall shape for the new contraction. Other design considerations dictated a contraction ratio of about eight with a 2-D (or at most mildly 3-D) contraction. The main requirements were that a laminar boundary layer at low Re_θ (less than about 500) is obtained at the splitter plate edge at reasonable flow speeds (10 - 20 m/s). This of course implies that the contraction length must be minimized. This was in addition to the usual requirements of wanting to avoid boundary layer separation on the walls and obtaining a reasonable mean flow uniformity at the contraction outlet (less than 1% nonuniformity). After an extensive review of the existing literature on contraction design, four polynomial

shapes were selected for testing with the new computational scheme: Third Order Polynomial, Fifth Order Polynomial, Seventh Order Polynomial and Matched Cubics. The contraction area ratio and cross-section, together with the inlet and outlet dimensions had already been decided by other considerations. The contraction area ratio was fixed at a value of 7.7, contracting from overall inlet dimensions of 91 × 274 cm to 91 × 36 cm. The optimization process, therefore, consisted of choosing the ideal contraction wall shape and length.

After running computations on a variety of designs, it was found that the minimum acceptable L/H_i for our requirements was 0.89, giving a length of 2.4 m. This particular length to height ratio was therefore used as a test case for all the contraction wall shapes. The contraction wall shape satisfying most of the requirements discussed above was the one given by the 5th order polynomial. It was free of separation (both on the centerline and in the corners) and gave a reasonable Re_θ ($\sim$ 400) and flow uniformity (better than 0.5% variation) at the operating conditions (U_e = 15 m/s). This wall shape was therefore used on the contraction for the mixing layer wind tunnel (Fig. 2).

The contraction is split into two identical two-dimensional contraction sections, each with an area ratio of 7.7. The contraction sections are mirror-images, mounted side-by-side, and separated by a splitter plate. The splitter plate separating the contractions tapers from 5 cm thick at the base to 0.5 mm thick at the trailing edge. The included angle thus formed is about 1.1°. The splitter plate protrudes 15 cm into the test section in order to allow some distance for streamline curvature to relax after the flow has passed through the contraction section, and to allow some recovery distance, should it be desired to trip the splitter plate boundary layers.

2.5 Test Section

Test section design is totally dependent on the requirements of the particular experiments to be performed in the wind tunnel. Blower tunnels are generally more flexible in accepting a wide variety of test sections, both with and without exit diffusers. The flow out of a contraction often takes a short distance (equivalent to about 0.5 diameters) before the flow nonuniformities and angularities are reduced to an acceptable level. Also, if a turbulence grid is installed at the test section inlet, it may take up to 10-15 mesh lengths before a homogeneous flow is obtained. These requirements often fix the minimum length of the test section. General purpose test sections normally have cross-sectional aspect ratios of approximately 1.5:1. However, tunnels designed for shear layer research normally have test sections with a width-to-height ratio of at least five. The main requirement, in this case, is that a reasonable thickness of irrotational flow remains between the shear layers by the end of the test section.

The present test section is totally constructed out of plexiglas and has the dimensions of 36 cm in the cross-stream direction, 91 cm in the spanwise direction, and 3.7 m in length. Since the contraction sections lie side-by-side, the mixing layer is oriented vertically. The overall test section aspect ratio is AR = 2.5; each half has an aspect ratio of just over five. It is more useful, however, to compare the size of the tunnel with the thickness of the shear layer being studied. In the case of a two-stream mixing layer of velocity ratio 0.6, the maximum measured layer thickness (at 2.5 m downstream) was 11 cm (Bell and

Mehta, 1989b). So the spanwise extent of the mixing layer at this point was 8.3 times the mixing layer thickness, thus ensuring at least *geometric* two-dimensionality. By this station, the high- and low-speed sidewall boundary layers were about 2.5 cm thick, leaving a 10 cm potential flow core on each side of the mixing layer. The test section flow exhausts into the laboratory; there is no diffuser at the downstream end. Static pressure ports are drilled at 61 cm intervals in the test section bottom wall, roughly along the mixing layer centerline to monitor the streamwise pressure gradient. The sidewall on the low-speed side is movable and flexible, and can be adjusted to give a prescribed pressure gradient.

The low-speed sidewall consists of a number of removable plexiglass sheets. The sheets can be bolted together in a variety of configurations, and are held in place with toggle clamps which press against the sidewalls. The test section sidewalls extend outward on the low-speed side beyond the edge of the contraction section, forming a shelf on which the movable wall rests. The movable wall can be adjusted to any desired position and then locked in place with the toggle clamps; this enables the streamwise pressure gradient to be set to within $< 1\%$ of the dynamic pressure. One section of the movable wall has a series of spanwise slots cut into it. The slots are 1.6 cm wide and cover the center 76 cm of the wall. When not in use, the slots are closed with plexiglass plugs. By altering the movable wall configuration, probe access can be obtained at 7.6 cm intervals along the entire length of the test section.

3. WIND TUNNEL PERFORMANCE

A study was undertaken to analyze the performance of the mixing layer wind tunnel. The flow was assumed to be one-dimensional, steady and adiabatic. Furthermore, skin friction losses on the wind tunnel walls were neglected and empirical correlations were used to estimate the losses through the various wind tunnel components. The blower specifications were obtained from the manufacturer's charts. The main pressure losses incurred by the flow are through the screens and the honeycomb. Wieghartdt's (1953) formula (Eqn. 1) was used to estimate the pressure drop through the screens while Loerke and Nagib's (1972) experimental data were interpolated to give the pressure losses through the honeycombs. There is an additional loss equivalent to the test section total head due to the absence of an exit diffuser. The measured performance of the two legs of the wind tunnel were then compared to the predicted performance over some selected ranges of operation.

Figures 3 and 4 show the static pressure rise and brake horsepower plotted as a function of the flow rate for selected (constant) values of the blower RPM. These curves are plotted for both blowers from the performance charts supplied by the manufacturer.

The RPM, pressure rise and power required by the blowers are plotted as a function of the flow rate (CFM) in Figs. 5, 6 and 7. Since the pressure drop coefficients of the screens and honeycombs are only weak functions of the Reynolds number, the functional relationships in Figs. 5, 6 and 7 should be first, second and third order, respectively, as is broadly the case. The measured RPM and power and are also compared with the predicted values in Figs. 5 and 7. The agreements are generally quite good, with the

actual performance somewhat lower than predicted. This is not too surprising since not all of the possible losses through the wind tunnel components have been accounted for in the present analyses.

For the maximum test section flow speeds of 20 m/s and 40 m/s on the low- and high-speed sides of the wind tunnel, respectively, the CFMs are 7,000 and 15,000 giving RPMs of about 1300 and 1100, blower pressure rises of 1 inch and 4 inches and HPs of 2 and 15, respectively.

4. WIND TUNNEL FLOW CALIBRATION

4.1 Mean Flow Uniformity

The reasons for desiring a uniform core flow in a wind tunnel test section are obvious. Spatial non-uniformity of the mean velocity within the test section can be caused by asymmetric boundary layer growth or separation in one of the wind tunnel legs, or by a persisting asymmetric flow produced by the fan or blower. In a return-circuit wind tunnel, poor corner vane design can also lead to mean flow nonuniformity. The acceptable levels for mean flow uniformity are generally at least five times the r.m.s. turbulent fluctuation levels sought in a high quality wind tunnel. The flow conditioning installed in modern wind tunnels, such as a honeycomb, screens and a contraction with a reasonable area ratio, improves both the mean flow uniformity and the turbulence intensity levels. Therefore, fulfilling the low turbulence requirements will almost always ensure an acceptable level of mean flow uniformity as well (Bradshaw and Pankhurst, 1965).

The mean flow uniformity in the test section was measured by scanning a pitot tube over portions of the potential core region. The flattened pitot tube with dimensions of about 0.5×1.0 mm and a local static port were connected to a Datametrics Inc type 511-10 barocell pressure transducer, with its associated amplifier and signal conditioner. The pressure transducer range was 0-10 mm Hg, corresponding to a velocity range of 0-47 m/s. For the mean flow uniformity measurements, the pressure transducer signal was first directed through the Precision Buck & Gain unit (typically set to a DC offset of 1 volt and a gain of 10) to expand the range and provide greater resolution with the A/D. The pressure reading at each point was averaged over 1750 samples obtained at a rate of 150 samples/second. The pressure transducer was calibrated against a Combist Precision Manometer, which had a range of 2.2 mm Hg and an accuracy of 0.00015 mm Hg. Pitot probe dynamic pressure data were reduced to velocity data by the FMDAS software (Hooper and Saunders, 1986), using the local temperature input by the operator.

A typical example of the measured mean velocity variation is shown in Fig. 8 in the form of contour plots. The maximum variation of the mean streamwise velocity is less than $\pm$ 0.25%. This level of uniformity was found to exist throughout the test section within the potential core regions, in the regions away from the shear layers.

The mean flow angularity was obtained from the cross-wire measurements which were primarily conducted to evaluate the turbulence levels in the wind tunnel. Some typical measurements of the cross-flow velocities made in the free-stream are presented in Fig.

9. The normalized cross-flow velocities (V/U_e and W/U_e) were generally found to be less than ± 0.005; corresponding to a flow angularity of less than 0.25°.

4.2 Boundary layer and Spanwise Skin Friction Measurements

As in the present case, aspect ratios of five to six are typically used for test-sections in which a two-dimensional boundary layer is desired. However, it is now widely known that a uniform core-flow and a large aspect ratio does not necessarily guarantee a two-dimensional boundary layer. Large, quasi-periodic spanwise variations (20% or more) in boundary layer thickness, surface shear stress and turbulence intensity are often encountered in what is assumed to be a two-dimensional boundary layer (Bradshaw, 1965). Over the years, several researchers have observed and studied this spanwise variation (see Mehta and Hoffmann, 1986 for a review). It has been attributed to a spatial instability which causes directional changes in the jets emerging from the pores of screens. The spatial instability leads to the formation of weak longitudinal vortices in the boundary layer. Longitudinal vortices, once formed, persist for long distances downstream, even in a turbulent boundary layer, and are effective at producing significant spanwise variations in surface shear stress. Since the local changes in flow direction are small and hence difficult to measure, the quantity most suited for this check is the spanwise surface shear stress, which is adequately measured by traversing a Preston tube across the test-section floor.

In order to determine the two-dimensionality of the boundary layers on the splitter plate in the present wind tunnel, the spanwise surface shear stress distributions were measured for both untripped and tripped conditions. For the tripped cases, 2.5 cm wide roughness strips comprising of a random distribution of round glass beads were installed 20 cm upstream of the splitter plate trailing edge. The beads used on the high-speed side had an average diameter of about 0.75 mm, whereas those for the low-speed side had an average diameter of about 1 mm. All the measurements of the boundary layer properties and surface shear stress were made with a 0.5×1 mm pitot tube. For the surface shear stress measurements, the front end of the pitot tube was placed on the splitter plate surface (acting as a Preston tube) before collecting the data. Contact between the pitot tube and the splitter plate was assured by completing an electrical circuit. Data acquisition and reduction procedures were the same as for the mean flow uniformity measurements described above in Section 4.1.

The boundary layer properties measured on the splitter plate centerline and about 1.2 cm upstream of the trailing edge are presented in Table 1 for both, the tripped and untripped cases. The repeatability in the measured boundary layer properties was generally better than 2%.

The spanwise distributions of the surface shear stress are presented in Figs. 10 and 11. The results are plotted in the form of the surface dynamic pressure reading normalized by the centerline value. The surface pressure reading is proportional to ${C_f}^2$ for laminar boundary layers and proportional to ${C_f}^{8/7}$ for turbulent boundary layers. Since the variation in spanwise surface shear stress is not significantly affected by Reynolds number (Mehta and Hoffmann, 1986), the fact that the flow speeds for the various cases are not the same is expected to have minimal effect on the conclusions.

The laminar boundary layer results shown in Figs. 10a and b show a larger and more systematic variation on the high-speed side of the splitter plate. The peak to peak variation of the surface pressure is about ±25% on the high-speed side with a wavelength of about 4 cm. The reasons for the difference between the two sides of the splitter plate are not obvious although it should be noted that the blowers supplying the air to the two sides are *not* identical. Also, the variation on the high-speed side is apparently not unusually large for *laminar* boundary layers (Wood, 1980). Boundary layer profiles measured on the centerline and at $Z = \pm$ 15 cm showed that the layer properties varied by less than 5% on the low-speed sied and by less than 10% on the high-speed side. Somewhat surprisingly, the results for the tripped case are comparable for the two sides (Figs. 11a and b). The maximum peak to peak variation on both sides is about ±5% which is within the acceptable limits given by Mehta and Hoffmann (1986) for turbulent boundary layers. Boundary layer profiles measured at three spanwise locations ($Z = 0, \pm$ 13 cm) showed a variation of well within 5%. Although a distinct wavelength is not apparent, a nominal average of 2 cm is obtained on the low-speed side after careful examination of the data. Some recent spanwise surface shear stress measurements, with the boundary layers tripped by round wire trips, showed comparable peak to peak variations, although the details were somewhat different. The spanwise surface shear stress measurements therefore show that the initial boundary layers are nominally two-dimensional on both sides of the splitter plate for both tripped and untripped conditions.

4.3 Turbulence Intensity Measurements

The effects of free-stream fluctuations on the development and structure of a turbulent shear layer are now well appreciated. For example, boundary layer transition is found to be extremely sensitive to disturbances in the free-stream (Saric, 1986). More relevant to the present interest is the fact that mixing layers have also been shown to be affected by these fluctuations. It has been suggested that the breakdown to three-dimensionality of the mixing layer structure may well be determined by the level of the free-stream disturbances (Chandrsuda et al., 1978 and Wood and Bradshaw, 1982).

Bradshaw and Pankhurst (1964) divided the free-stream fluctuations into two components, namely turbulence and unsteadiness. They defined unsteadiness as "a velocity fluctuation of low enough frequency to be noticeable on manometers and balances". The distinction between the two was based on the sources of the irregularities — unsteadiness may be caused by an intermittent separation whereas "true" turbulence is generated by boundary layers and wakes of fan blades, for example. Wood and Westphal (1987) further split the unsteadiness into a one-dimensional (1-D) axial motion produced by, say the rotation of the fan or blower and the three-dimensional (3-D) unsteadiness which could be due to flow separation in some part of the wind tunnel. In most well designed wind tunnels where great care is taken to avoid boundary layer separations, the latter contribution may be ignored. It follows then that the unsteadiness will only contribute to $\overline{u'^2}$; the difference between $\overline{u'^2}$ and $\overline{v'^2}$ or $\overline{w'^2}$ can then be attributed to unsteadiness. It is therefore important to measure *all* the components of turbulence intensity and, in particular, without high pass filtering so that the low frequency unsteadiness is also captured in the measurements. Also, the measurements should be made at several locations within the test section so that

regions of local production, if any, and the importance of induced motions (potential flow fluctuations) from the shear layers are realized (Wood and Westphal, 1987).

The present turbulence intensity measurements were made using a crossed hot-wire probe held on a 3-D traverse and linked to a fully automated data acquisition and reduction system controlled by a MicroVax II computer. The crossed hot-wire probe had 5 μm tungsten sensing elements about 1 mm long and positioned about 1 mm apart. The probe was calibrated statically in the potential core of the flow assuming a 'cosine-law' response to yaw, with the effective angle determined by calibration (Westphal and Mehta, 1983). The only filtering of the analog signals was to low pass filter at 30 Khz to provide immunity from high frequency electronic noise; the spectral measurements showed that all of the free-stream fluctuations resided well within this cut-off frequency. The analog signals were also DC offset, and amplified ($\times$10) before being fed into a NASA-built computer interface containing a fast sample-and-hold A/D converter with 12 bit resolution. The offset/gain procedure allowed the input signal to be matched to the $\pm$10 volt range of the A/D, in order to maximize resolution of the signal. The digital data were then multiplexed to the computer through a DMA board.

In the present free-stream measurements, for reasonable repeatability in the Reynolds stresses ($\sim$ 5%), it was found necessary to average the individual statistics over 50,000 samples obtained at a rate of 400 samples per second; the data were actually averaged over 10 individual data points each evaluated from 5,000 samples. Data were obtained in two planes (uv and uw) by rotating the crossed hot-wire probe about its own axis. This method yielded all three components of mean velocity, five independent components of the Reynolds stress tensor and selected higher order products.

Some preliminary turbulence measurements in the mixing layer wind tunnel with the sidewall positioned parallel to the fixed wall (i.e. normal mixing layer configuration) revealed that it was difficult to isolate the sources of the fluctuations because of "crosstalk problems" across the free-shear layer. The wind tunnel was therefore reconfigured such that each leg had its own test section; this was done by effectively extending the splitter plate all the way to the end of the test section. The two legs of the wind tunnel were then calibrated individually; some final checks with the test section in the normal (mixing layer) configuration were also made. The measurements were made in the Y and Z directions along the nominal centerlines of the individual test sections. Most of the data presented below were obtained at free-stream velocities of 9 and 15 m/s on the low- and high-speed sides, respectively.

The results for the low-speed side obtained at $X = 11$ cm are presented in Figs. 12a and b. The streamwise fluctuation ($\overline{u'^2}$) data from both planes (uw and uv) are presented for comparison. On the whole, reasonable agreement is observed between the results from the two planes with the uv-plane measurements slightly higher. There do not seem to be any systematic, significant variations in $\overline{u'^2}$ in either direction. The average ($\overline{u'^2}/U_e{}^2$) level is about 3×10^{-6}, which correponds to a turbulence intensity level, $u'/U_e \sim 0.17\%$. In the spanwise (Z) direction, the levels of $\overline{v'^2}$ and $\overline{w'^2}$ are comparable and much lower, as expected. Again, there is very little variation in the spanwise direction giving an average level for $\overline{v'^2}/U_e{}^2$ and $\overline{w'^2}/U_e{}^2$ of about 0.5×10^{-6}, which corresponds to $v'/U_e = w'/U_e \sim 0.07\%$. The results for these two components in the normal (Y) direction deserve more

comment. Both $\overline{v'^2}$ and $\overline{w'^2}$ are found to increase as the outer wall is approached, with $\overline{v'^2}$ increasing more rapidly. This is partly due to the induced fluctuations from the outer wall boundary layer and partly due to streamline curvature effects imposed by the contraction exit.

The measurements for the high-speed side (Figs. 13a and b) exhibit similar qualitative trends. The average $\overline{u'^2}/U_e{}^2$ level is somewhat lower at 2×10^{-6}, corresponding to $u'/U_e \sim 0.14\%$. The $\overline{v'^2}$ levels are slightly higher than the $\overline{w'^2}$ levels in both directions. The average $\overline{v'^2}/U_e{}^2$ level in figure 11a is still about 0.5×10^{-6}, whereas the $\overline{w'^2}/U_e{}^2$ level is slightly lower at 0.25×10^{-6}. Once again, the turbulence levels are found to increase in the Y-direction as the outer wall is approached with $\overline{v'^2}$ increasing more rapidly.

The measured turbulence levels on both sides of the mixing layer wind tunnel were well within the design specifications of $u'/U_e \leq 0.2\%$. As discussed above, the measured u'/U_e levels of approximately 0.15% in both legs of the wind tunnel include contributions from the low frequency unsteadiness; the "true" turbulence levels are approximately half that (0.07%).

4.4 Spectral Measurements

Although the turbulence intensity levels were found to be adequately low in the mixing layer wind tunnel, some spectral measurements were made to investigate the nature or frequency content of the unsteadiness contributions in the hope of identifying its sources.

The signal from a single hot-wire was examined with a digital spectrum analyzer to characterize dominant frequencies of velocity fluctuations within the free stream. The output of the hot-wire anemometer was connected directly to the spectrum analyzer, so that a hot-wire voltage spectrum, rather than a velocity spectrum, was obtained. Nevertheless, the location and relative amplitude of frequency peaks should correspond. Frequency peak measurements were made by surveying the entire frequency spectrum, choosing the ranges which most accurately displayed any peaks found, and photographing the display with a Polaroid camera. The frequency range was not changed when measurements of relative amplitude were made, to avoid bandwidth effects on the amplitude. The measurements were made over a wide range of flow speeds, and hence blower RPMs, on both sides of the wind tunnel since the blower fan is the most obvious source of fluctuations. The speed range covered, and the corresponding blower RPMs and blade passing frequencies are tabulated in Table 2.

Figure 14 shows the results for the low-speed side while those for the high-speed side are presented in Fig. 15. On both sides, and at all speeds, the most predominant (highest) peak occurs at the frequency corresponding to the revolutions per second. The blade passing frequency is not apparent in any of the results, although the results for the lowest flow speed ($U_e = 5$ m/s) show the presence of some extraneous peaks. The once per revolution unsteadiness is probably caused by a slight misalignment of the impeller which cannot be easily adjusted. Since the tubulence levels were within acceptable limits, no attempts were made to rectify this situation.

5. CONCLUDING REMARKS

A new wind tunnel, specifically designed for mixing layer experiments, has been constructed and calibrated. The unique feature of the tunnel is that it is driven by two separate blowers which feed two legs separated up to the test section where the two streams are allowed to merge. The mean flow in the test section is uniform to within $\pm 0.25\%$ and the flow angularity is less than $0.25°$. The spanwise variation of the surface shear stress is less than $\pm 5\%$ for the tripped boundary layers on the splitter plate indicating acceptable two-dimensionality. The total streamwise free-stream turbulence intensity level is approximately 0.15% with the cross-stream components equal to about 0.07%. The spectral measurements indicate that the main source of unsteadiness is the once per revolution contribution from the blower impeller. So overall, the wind tunnel flow quality is considered to be well within specifications and experiments designed to investigate the three-dimensional structure of plane mixing layers (Bell and Mehta, 1989b) and wakes are already being conducted in this facility.

ACKNOWLEDGEMENTS

We are grateful to Mat Russo of Oliver Johnson for his careful supervision of the tunnel component construction and to David Yaste for considerable help in assemblying the wind tunnel. We would also like to thank Susan Praskins for the test section fabrication and Bruce Wu for conducting the tunnel performance calculations. Helpful discussions with David Wood during the calibration phase are also gratefully acknowledged.

This work was supported by the Fluid Dynamics Research Branch at NASA Ames Research Center under grant NCC-2-55.

REFERENCES

Batchelor, G.K. "The Theory of Homogeneous Turbulence," *Cambridge University Press*, pp. 68-75, 1953.

Bell, J.H. and Mehta, R.D. "Contraction Design for Small Low-Speed Wind Tunnels," JIAA Report TR-64, Department of Aeronautics and Astronautics, Stanford University, April 1988. Also NASA CR-177488, August 1988.

Bell, J.H. and Mehta, R.D. "Boundary Layer Predictions For Small Low-Speed Contractions," *AIAA Journal*, Vol. 27, pp. 372-374, March 1989a.

Bell, J.H. and Mehta, R.D. "Three-dimensional Structure of a Plane Mixing Layer," Department of Aeronautics and Astronautics, JIAA TR-90, March 1989b. Also, AIAA Paper 89-0124, January 1989b.

Bradshaw, P. "Wind Tunnel Screens: Flow Instability and its Effect on Aerofoil Boundary Layers," *Journal of Royal Aeronautical Society*, Vol. 68, pp. 198, 1964.

Bradshaw P. and Pankhurst R.C. "The Design of Low-Speed Wind Tunnels," *Progress in Aerospace Sciences*, Vol. 5, p. 1, 1964.

Bradshaw, P. "The Effect of Wind Tunnel Screens on Nominally Two-Dimensional Boundary Layers," *Journal of Fluid Mechanics*, Vol. 22, pp. 679, 1965.

Bradshaw, P. "Two More Wind Tunnels Driven by Aerofoil-Type Centrifugal Blowers," Imperial College Aero Report 72-10, 1972.

Bradshaw, P. "Effects of Streamline Curvature on Turbulent Flow," AGARDograph 169, 1973.

Cebeci, T. and Bradshaw, P. "Momentum Transfer in Boundary Layers," Hemisphere Publishing Co., 1977.

Chandrsuda, C., Mehta, R.D., Weir, A.D. and Bradshaw, P. "Effect of Free-Stream Turbulence on Large Structure in Turbulent Mixing Layers," *Journal of Fluid Mechanics*, Vol. 85, pp. 693, 1978.

Dryden, H.L. and Schubauer, G.B. "Use of Damping Screens for Reduction of Wind Tunnel Turbulence," *Journal of the Aeronautical Sciences*, Vol. 14, p. 221, 1947.

Hooper, C. and Saunders, D. "FMDAS: Fluid Mechanics Data Acquisition System User's Guide," Technical Report 7104-3-7, Sterling Software, September 1986.

Laws, E.M. and Livesey, J.L. "Flow Through Screens," *Annual Review of Fluid Mechanics*, pp. 247-266, Vol. 10, 1978.

Loehrke, R.I. and Nagib, H.M. "Experimental Investigation on Management on Free-Stream Turbulence," AGARD Report 598, AD-749-891, 1972.

Mehta, R.D. "The Aerodynamic Design of Blower Tunnels with Wide-Angle Diffusers," *Progress in Aerospace Sciences*, Vol. 18, No.1, p.59-120, 1977.

Mehta, R.D. "Aspects of the Design and Performance of Blower Tunnel Components," Ph.D. Thesis, Department of Aeronautics, Imperial College, University of London, November 1978.

Mehta, R.D. and Bradshaw, P. "Design Rules for Small Low Speed Wind Tunnels," *The Aeronautical Journal*, Vol.83, No.827, November 1979.

Mehta, R.D. "Turbulent Flow through Screens," AIAA Paper 84-0538, January 1984.

Mehta, R.D. "Turbulent Boundary Layer Perturbed by a Screen," *AIAA Journal*, Vol. 23, No. 9, pp. 1335, September, 1985.

Mehta, R.D. and Hoffmann, P.H. "A Study of the Factors Affecting Boundary Layer Two-Dimensionality in Wind Tunnels," Department of Aeronautics and Astronautics, Stanford University, JIAA Report TR-66, 1986.

Mehta, R.D. and Hoffmann, P.H. "Boundary Layer Two-Dimensionality in Wind Tunnels," *Experiments in Fluids*, Vol. 5, No. 5, pp. 358-360, 1987.

Mokhtari, S. and Bradshaw, P. "Longitudinal Vortices in Wind Tunnel Wall Boundary Layers," *Aeronautical Journal*, Vol.87, 1983, pp. 233-236.

Morkovin, M.V. Observations of Streamwise Vortices in Laminar and Turbulent Boundary Layers. NASA Contractor Report 159061, April, 1979.

Patel, V.C. "Calibration of the Preston Tube and Limitations on its Use in Pressure Gradients," *Journal of Fluid Mechanics*, Vol. 23, pp. 185, 1965.

Prandtl, L. "The Attainment of a Steady Air Stream in Wind Tunnels," NACA-TM-726, 1933.

Saric, W.S. "Boundary Layer transition to Turbulence: The Last Five Years," Proceedings of the Tenth Symposium on Turbulence, University of Missouri, Rolla, Missouri, pp. 19-1:19-18, 1986.

Stratford, B.S. "The Prediction of Separation of the Turbulent Boundary Layer," *Journal of Fluid Mechanics*, Vol. 5, pp. 1-16, 1959.

Westphal, R.V. and Mehta, R.D. "Crossed Hot-Wire Data Acquisition and Reduction System," NASA TM-85871, 1983.

Wieghardt, K.E.G. "On the Resistance of Screens," *Aeronautical Quarterly*, Vol. 4, pp. 186, 1953.

Wood, D.H. "A Reattaching, Turbulent, Thin Shear Layer," Ph.D. Thesis, Department of Aeronautics, Imperial College, University of London, January 1980.

Wood, D.H. and Bradshaw, P. "A Turbulent Mixing Layer Constrained by a Solid Surface," *Journal of Fluid Mechanics*, Vol. 122, pp.265, 1984.

Wood, D.H. and Westphal, R.V. "Measurements of the Free-Stream Fluctuations Above a Turbulent Boundary Layer," NASA-TM 100036, November 1987.

Table 1 Boundary Layer Properties

Condition	U_e (m/s)	δ_{99} (cm)	θ (cm)	Re_θ	H	C_f $\times 10^3$
High-Speed Side, Untripped	15.0	0.398	0.0526	525	2.52	0.87
Low-Speed Side, Untripped	9.0	0.441	0.0606	362	2.24	1.56
High-Speed Side, Tripped	21.0	0.86	0.096	1301	1.49	3.99
Low-Speed Side, Tripped	10.5	0.87	0.098	686	1.53	4.85

Table 2 Flow Speed versus Blower Setting

Low-Speed Side		
U_e (m/s)	RPM	Rev/s
5	414	6.9
10	780	13.0
15	1160	19.3
20	1510	25.2

High-Speed Side		
U_e (m/s)	RPM	Rev/s
5	167	2.78
10	317	5.28
15	466	7.77
20	611	10.18

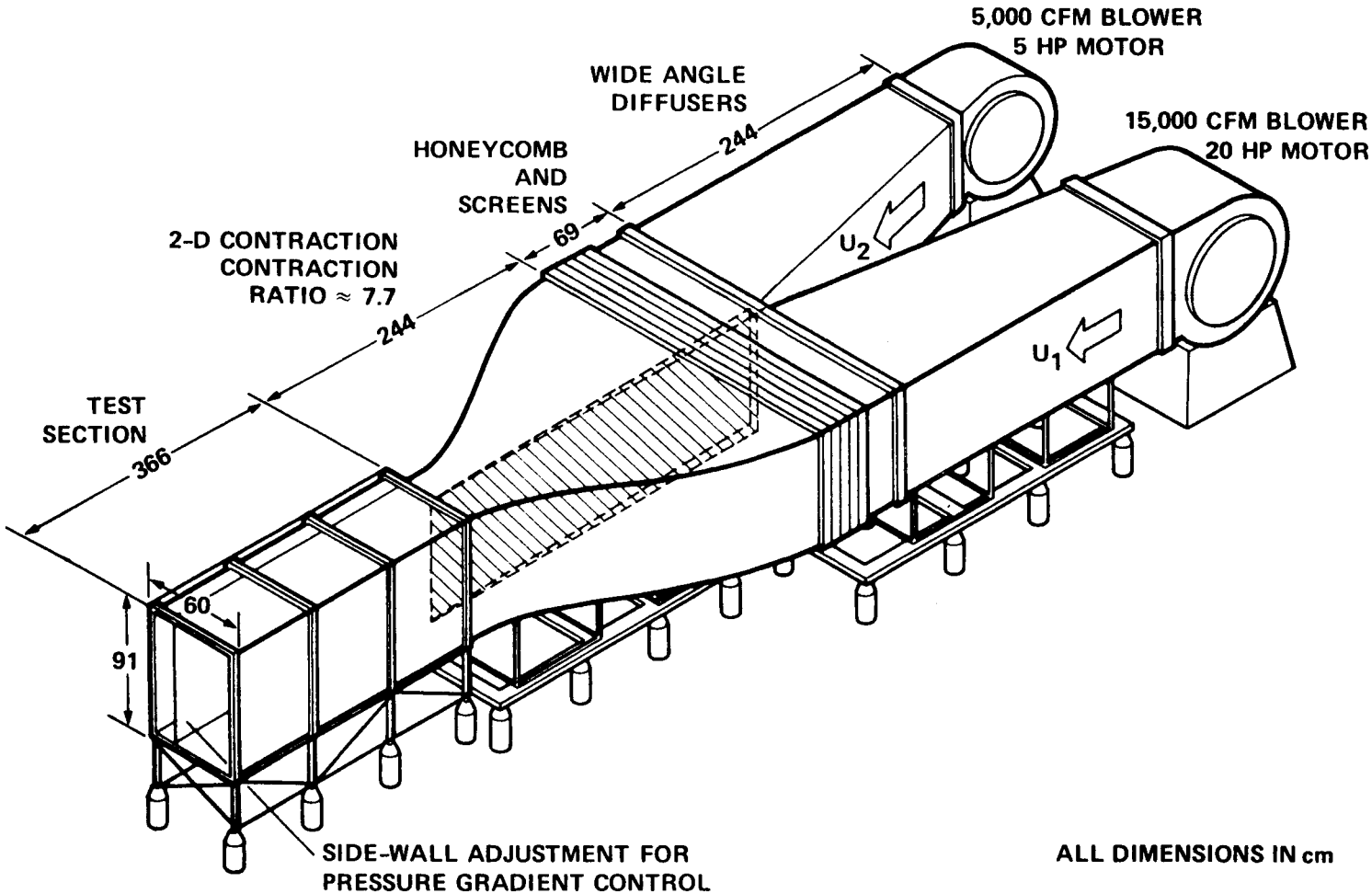

Figure 1. Schematic of Mixing Layer Wind Tunnel.

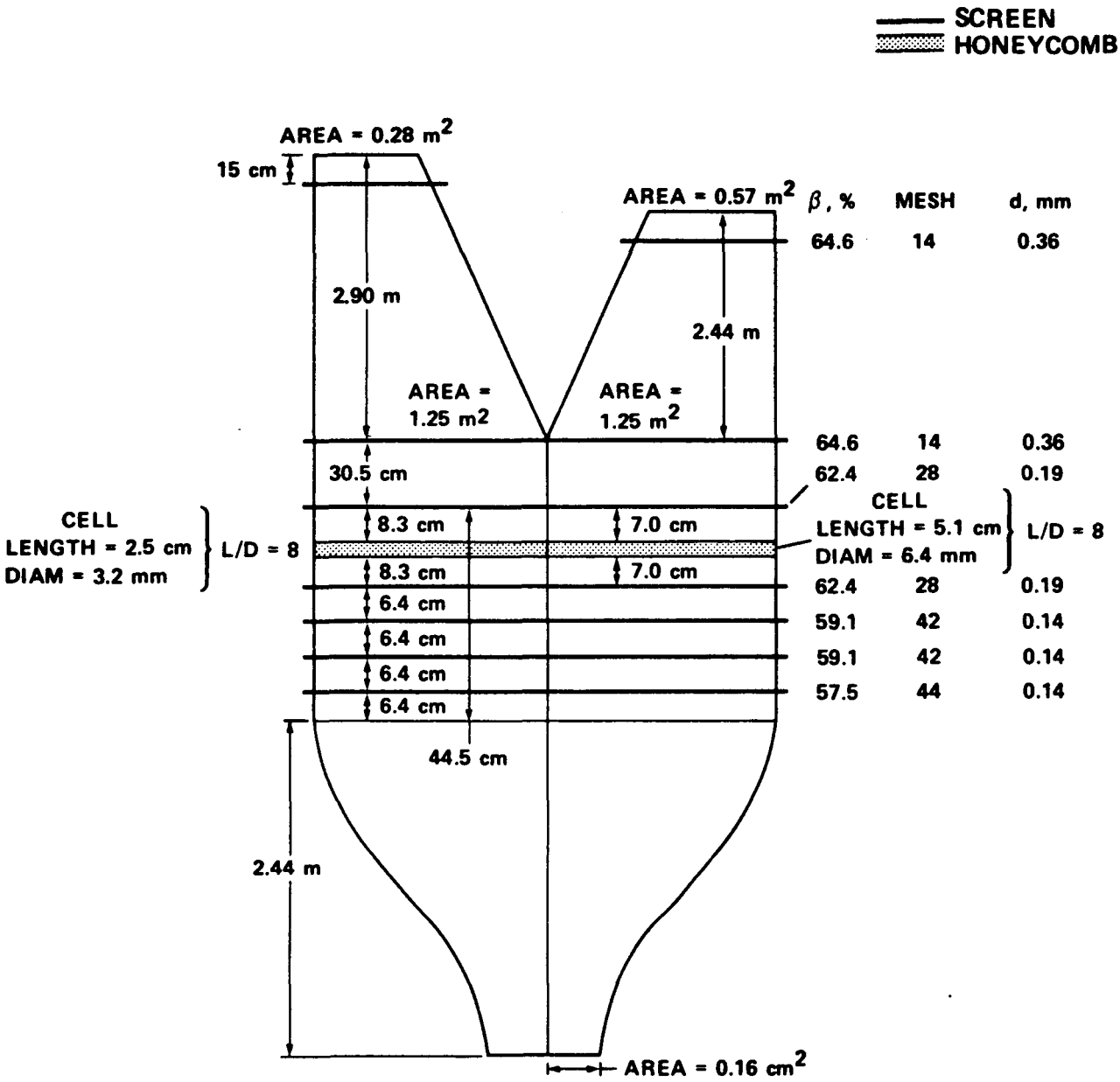

Figure 2. Block diagram of Mixing Layer Wind Tunnel, showing flow conditioning elements.

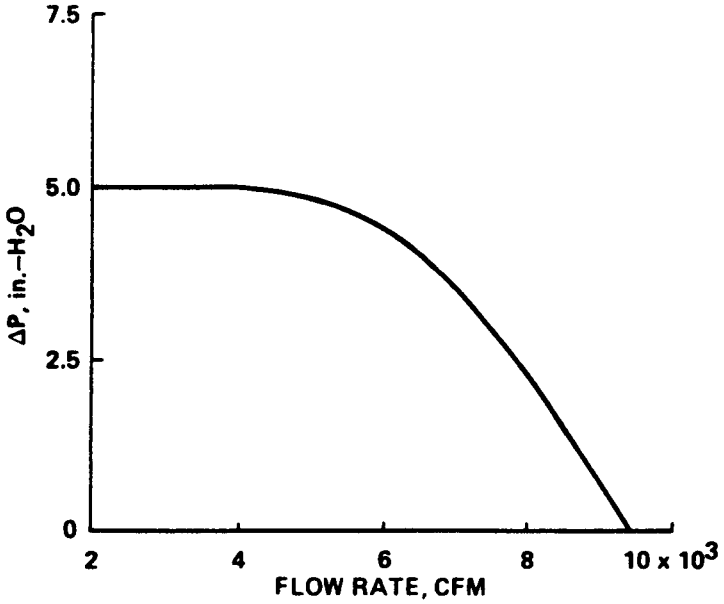

a) Low-Speed Side

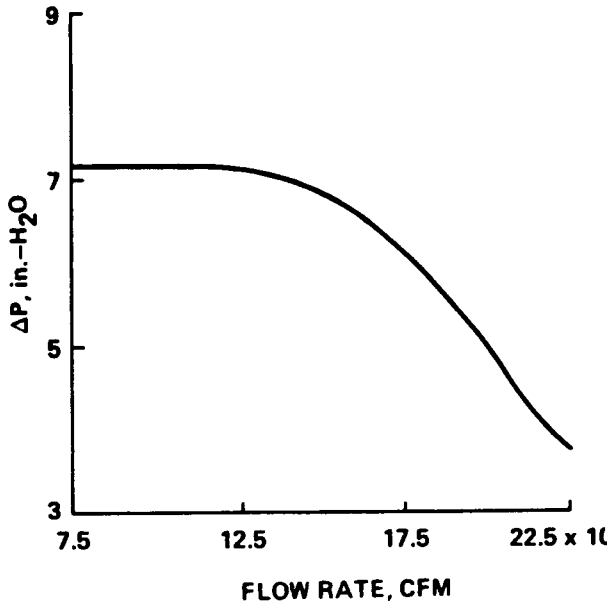

b) High-Speed Side

Figure 3. Static pressure rise versus flow rate (CFM).

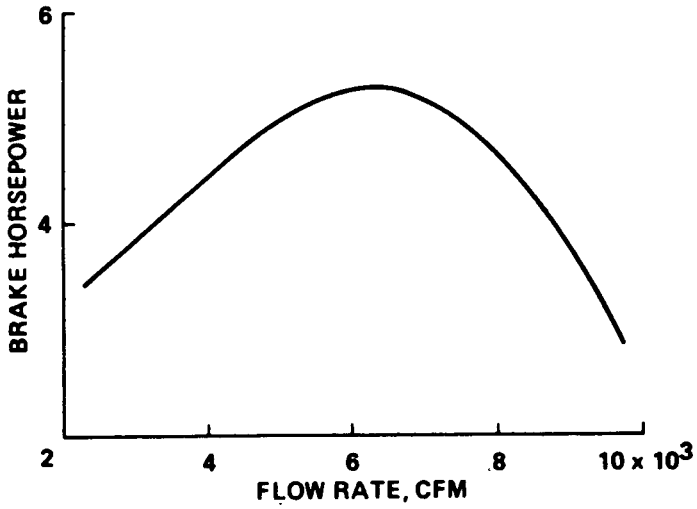

a) Low-Speed Side

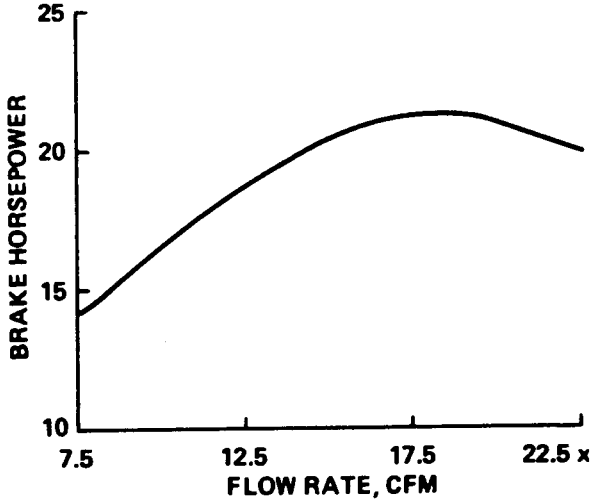

b) High-Speed Side

Figure 4. Brake horse power (BHP) versus CFM.

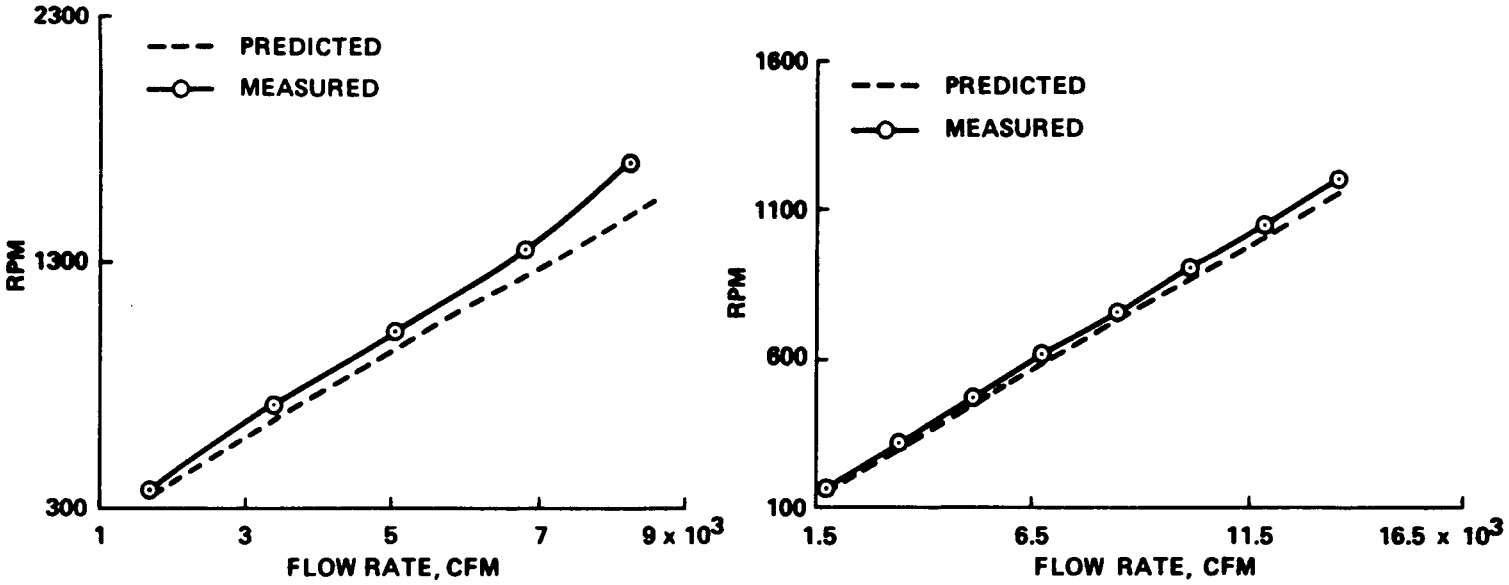

a) Low-Speed Side

b) High-Speed Side

Figure 5. Blower RPM versus CFM.

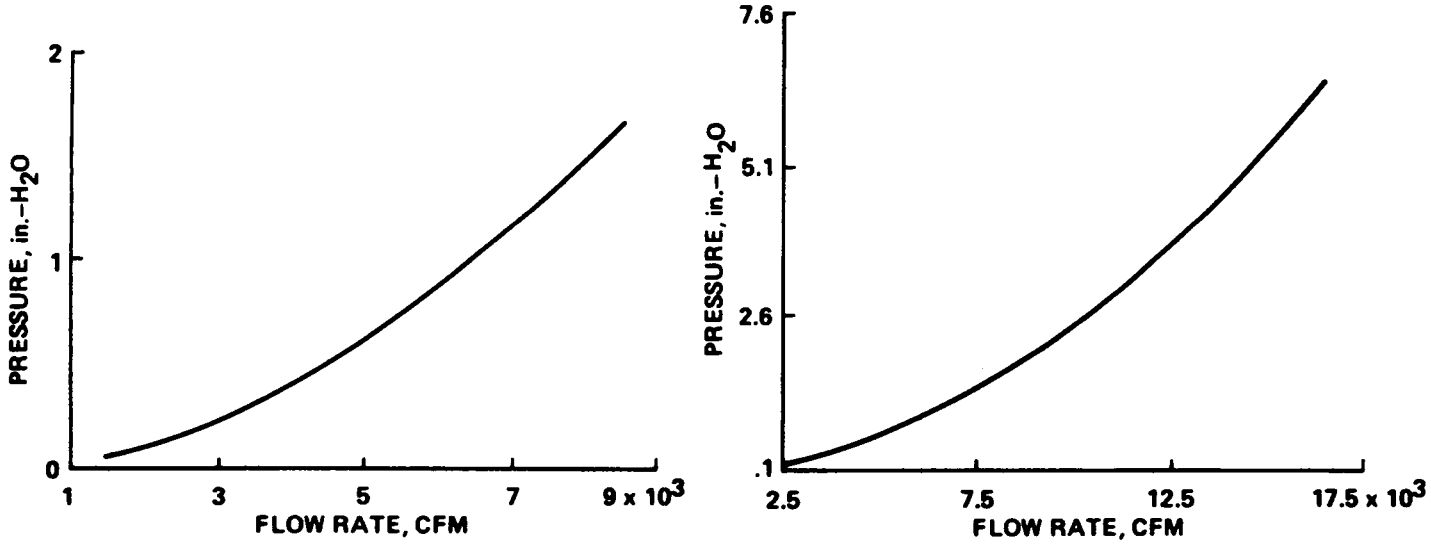

a) Low-Speed Side

b) High-Speed Side

Figure 6. Pressure rise versus CFM.

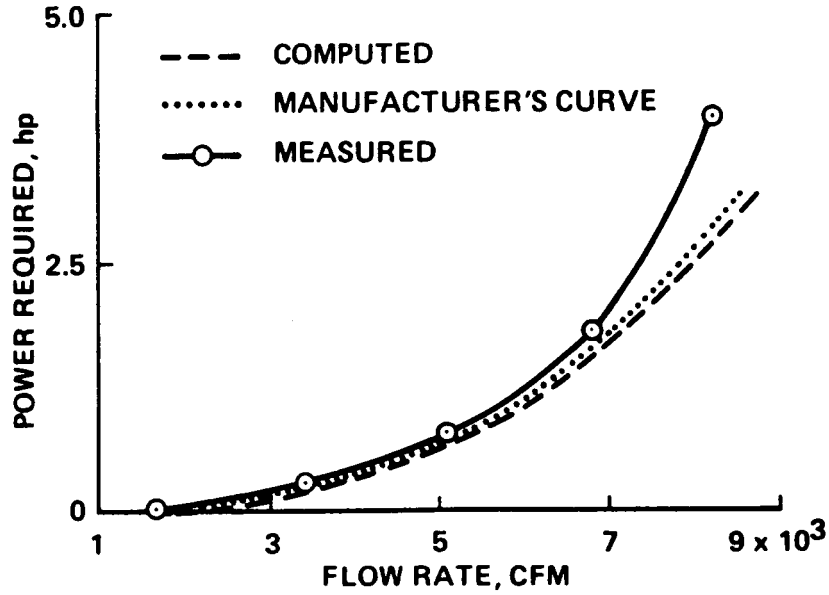

a) Low-Speed Side

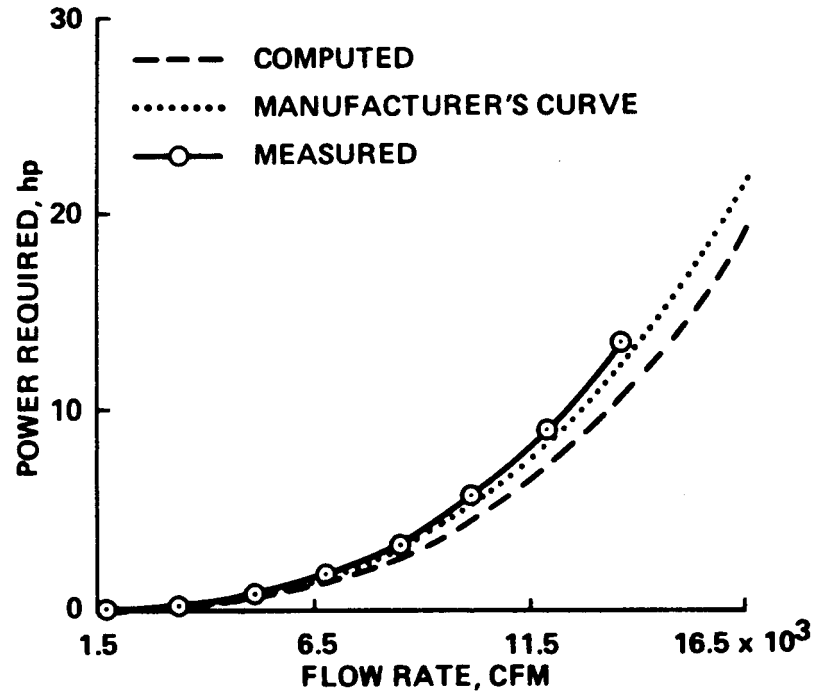

b) High-Speed Side

Figure 7. Work required by blower versus CFM.

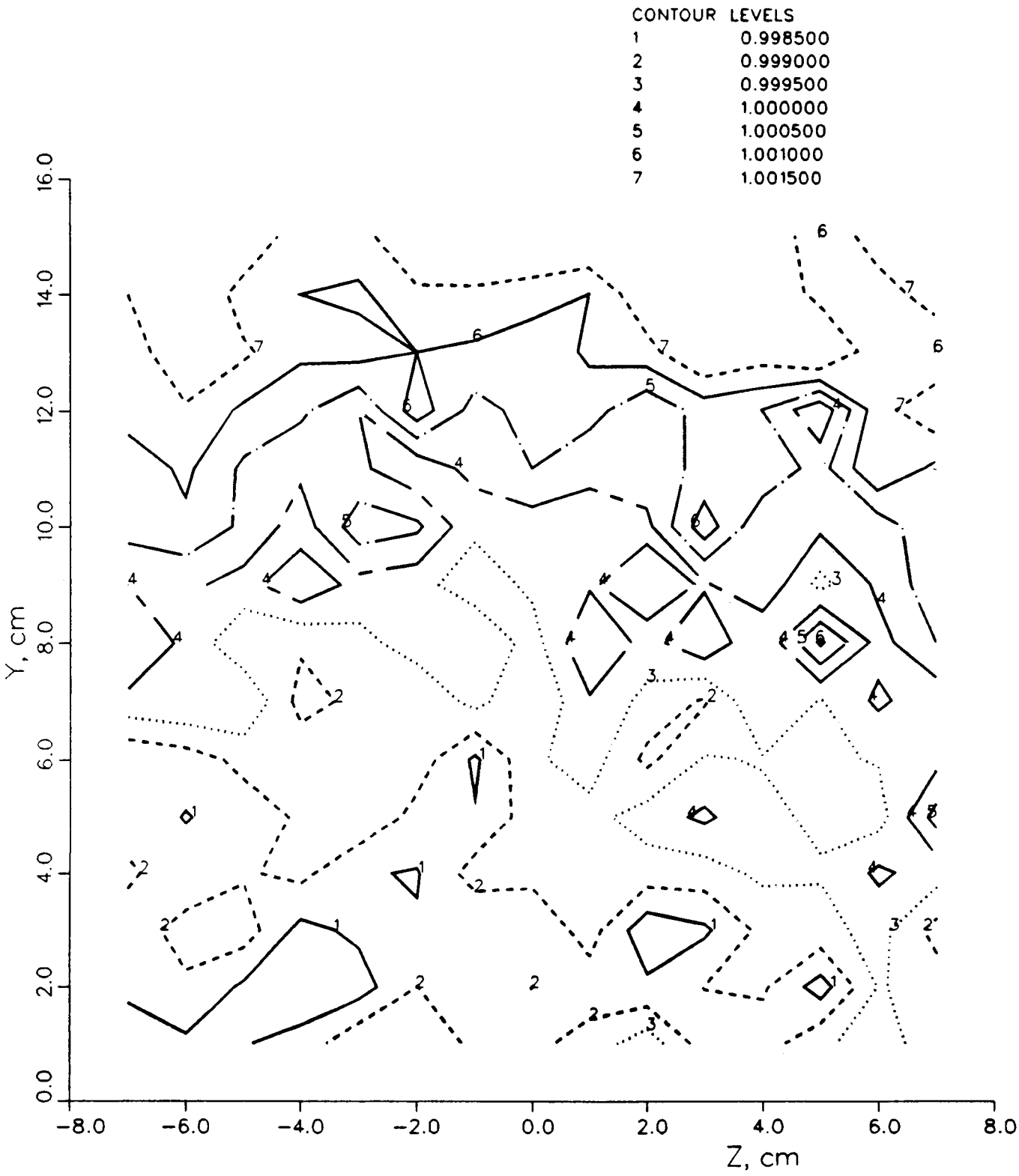

Figure 8. **Contour plot of mean flow uniformity. The levels have been normalized by the average velocity.**

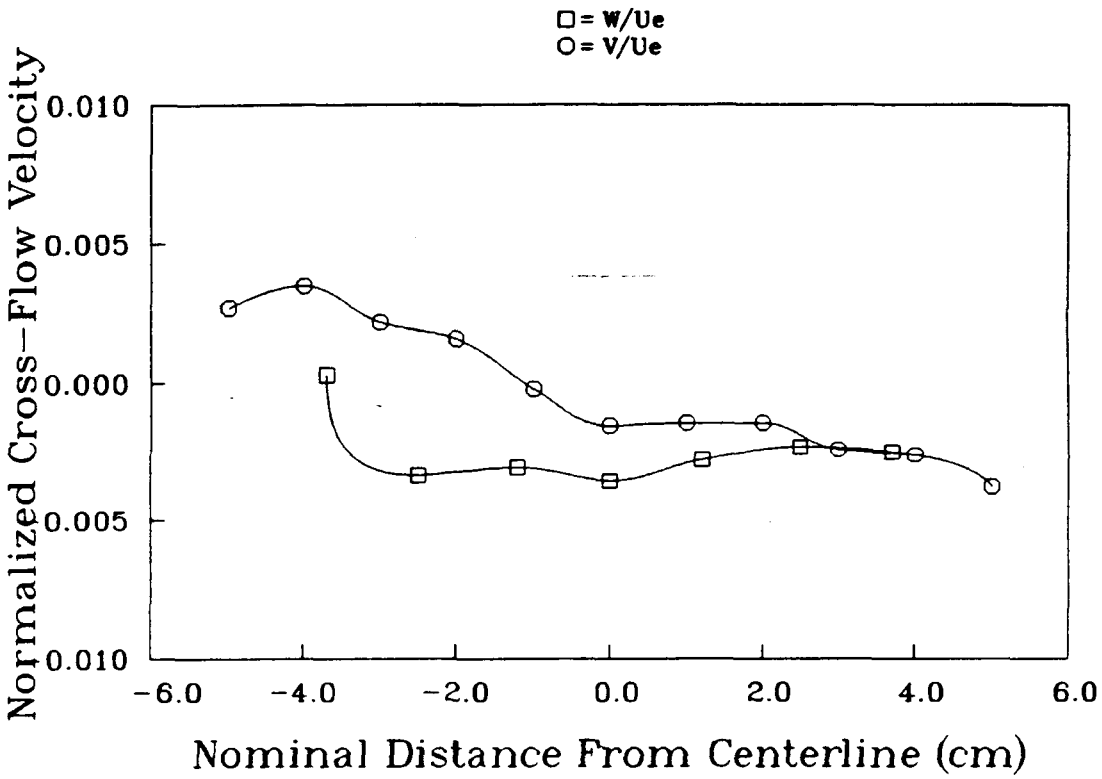

Figure 9. **Typical distribution of cross-flow velocities. The cross-flow velocities are measured along a line normal to the splitter plate, and are normalized by the average streamwise velocity.**

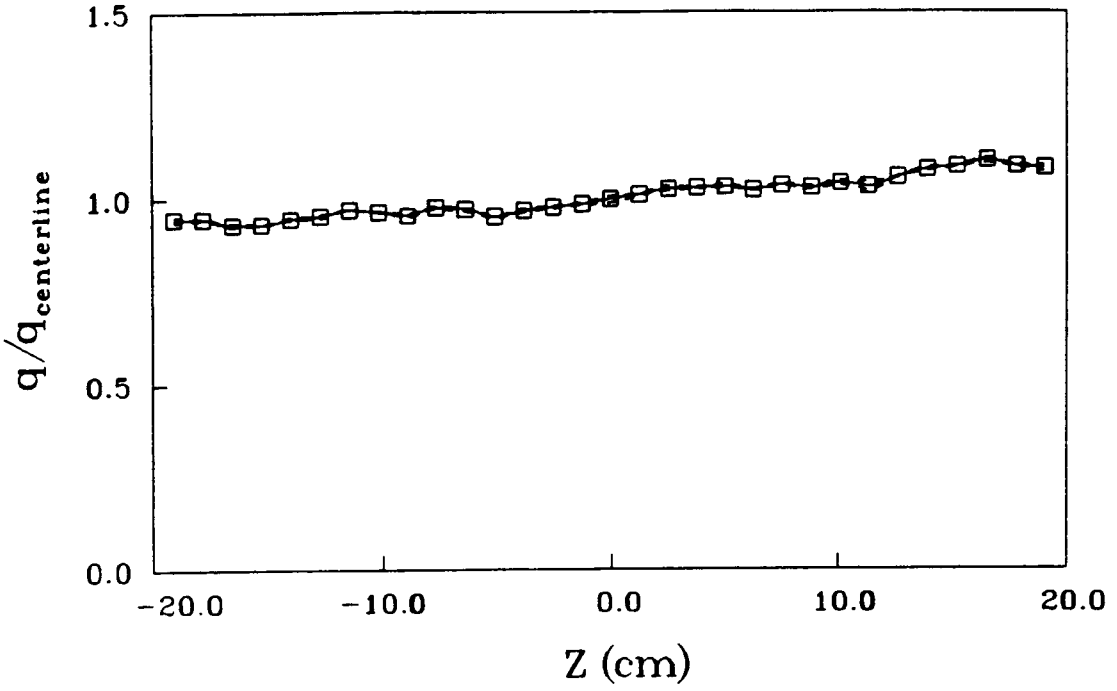

a) Low-Speed Side

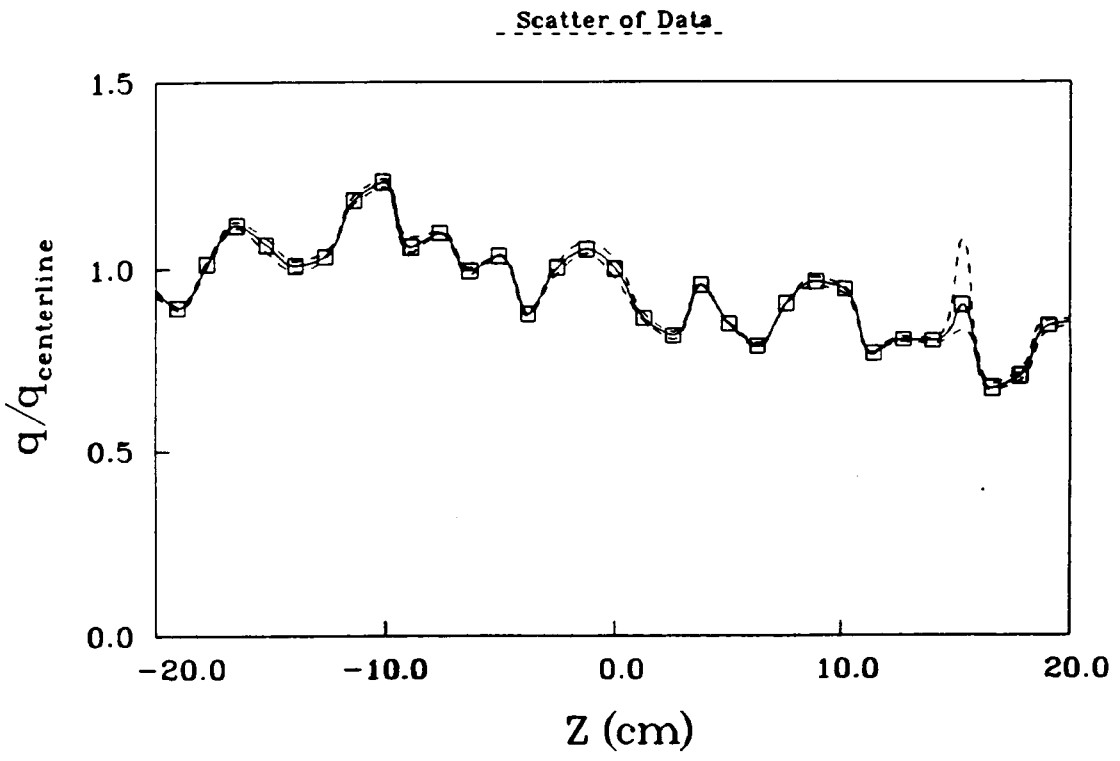

b) High-Speed Side

Figure 10. Spanwise distributions of surface shear stress for laminar (untripped) boundary layers

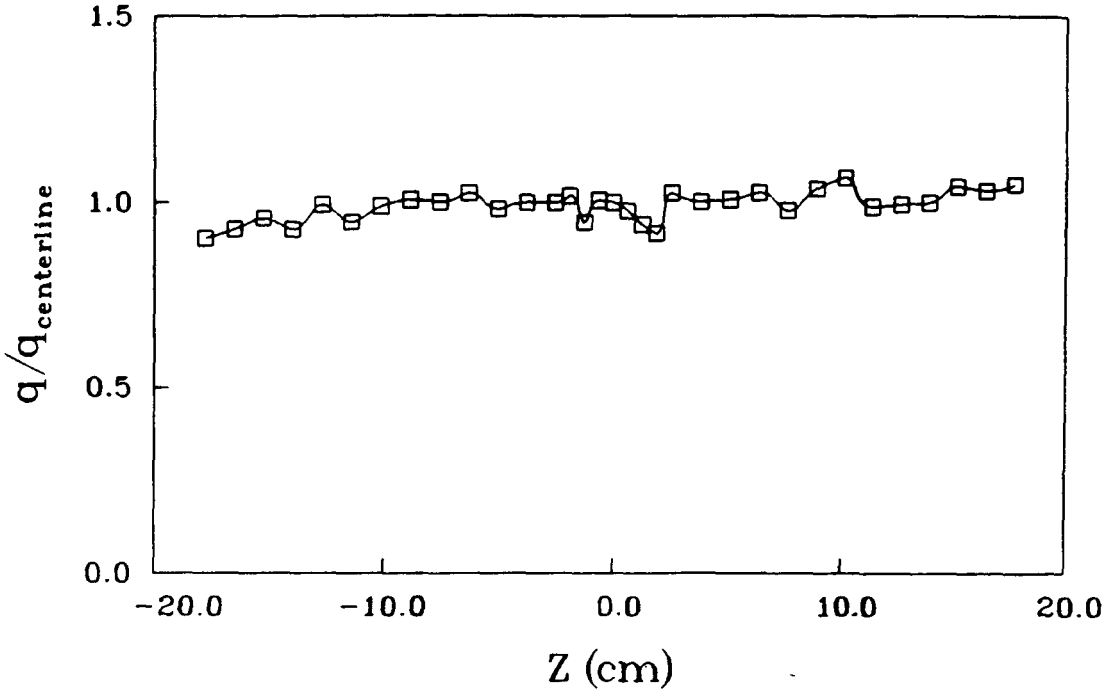

a) Low-Speed Side

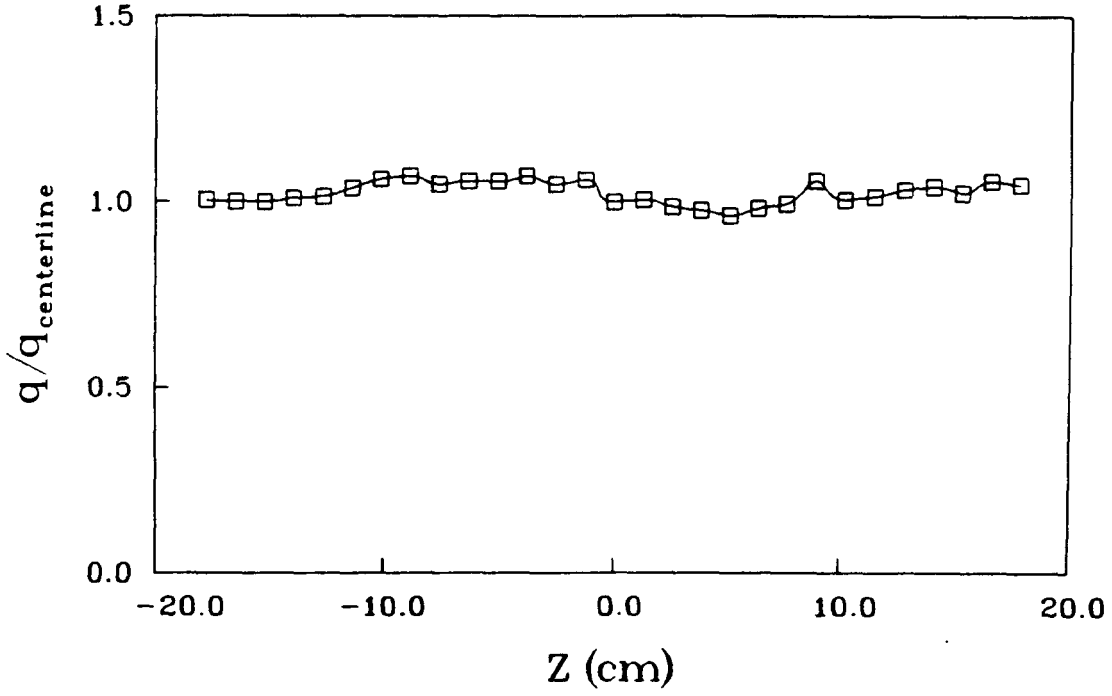

b) High-Speed Side

Figure 11. Spanwise distributions of surface shear stress for turbulent (tripped) boundary layers

Figure 12a. Turbulence intensity measurements on low-speed side. Data is shown along a line at X=11 cm, Y=5 cm.

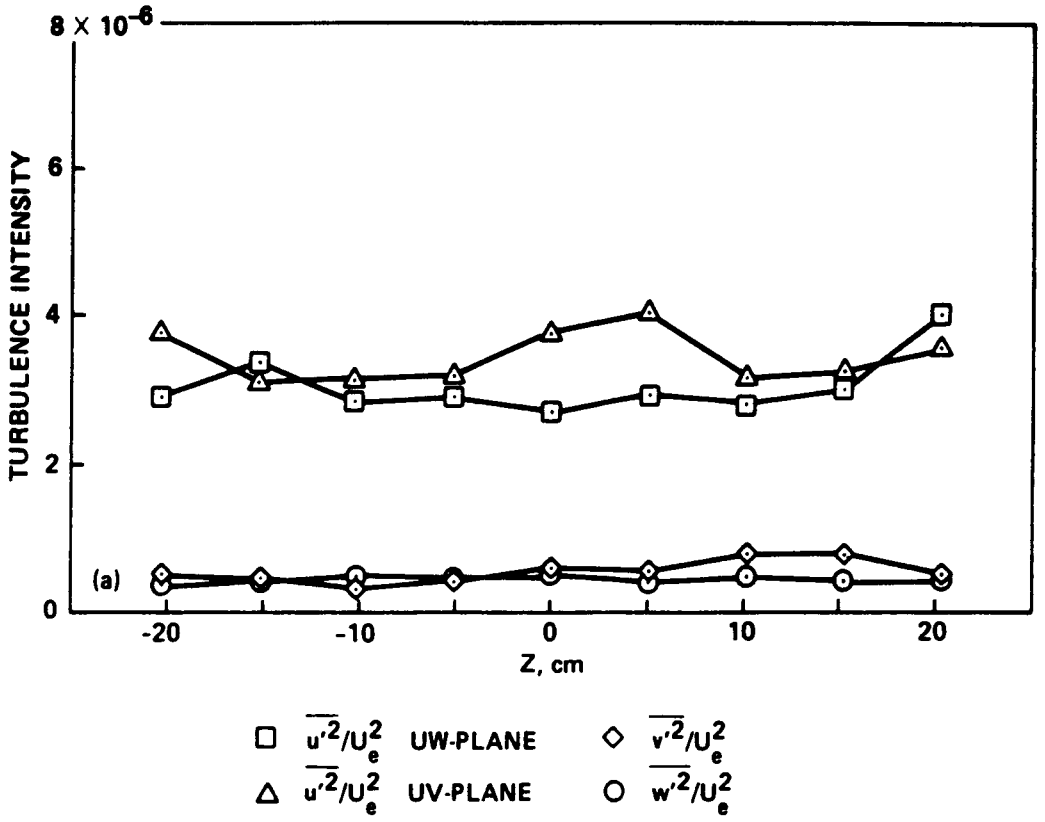

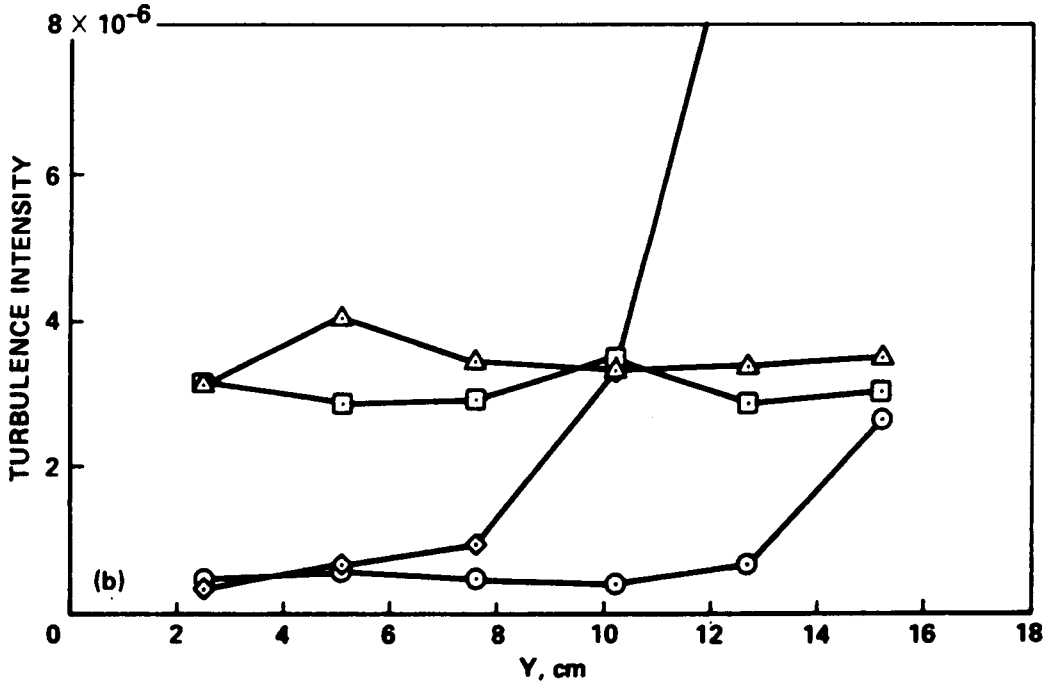

Figure 12b. Turbulence intensity measurements on low-speed side. Data is shown along a line at X=11 cm, Z=0 cm.

Figure 13a. Turbulence intensity measurements on high-speed side. Data is shown along a line at X=11 cm, Y=5 cm.

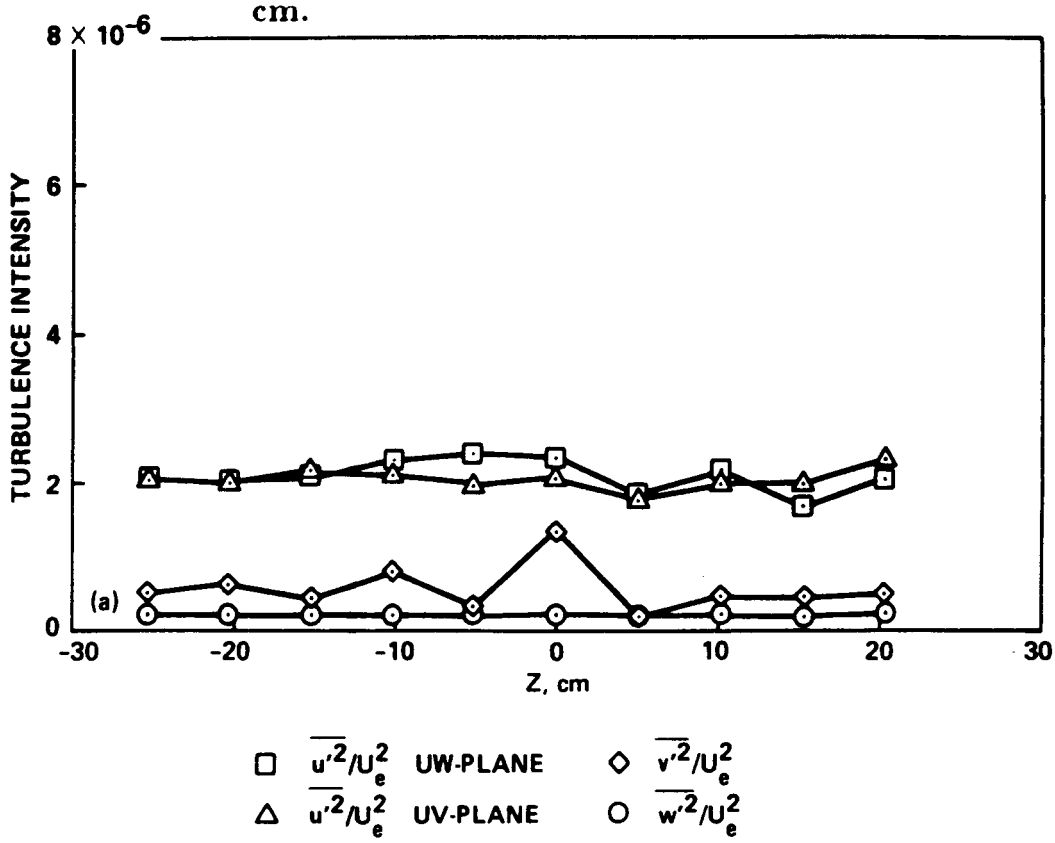

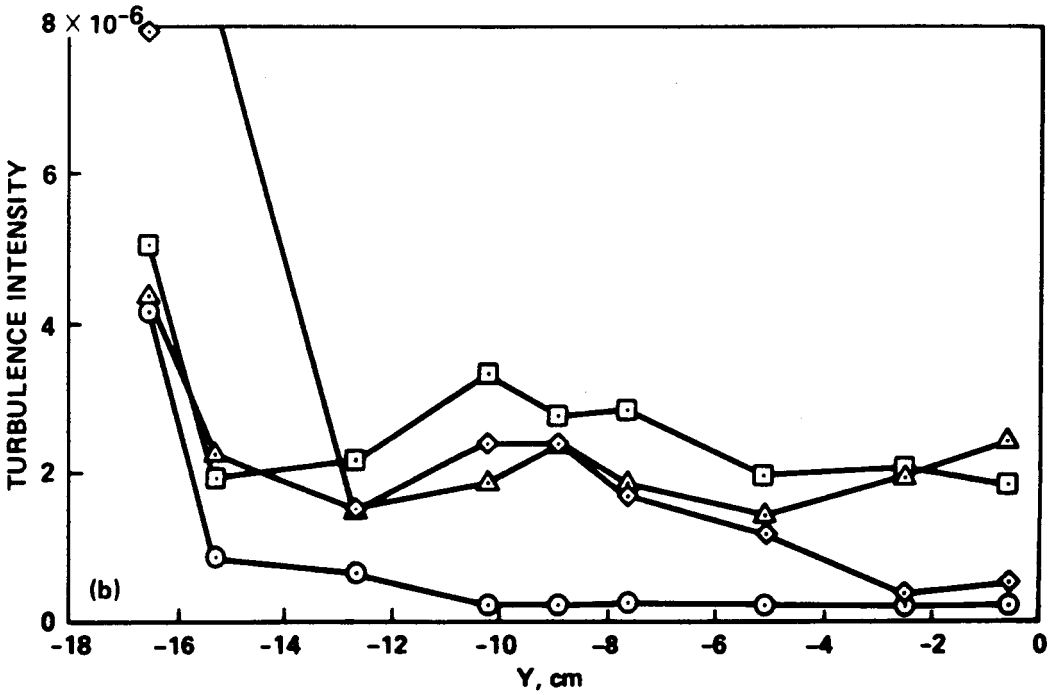

Figure 13b. Turbulence intensity measurements on high-speed side. Data is shown along a line at X=11 cm, Z=0 cm.

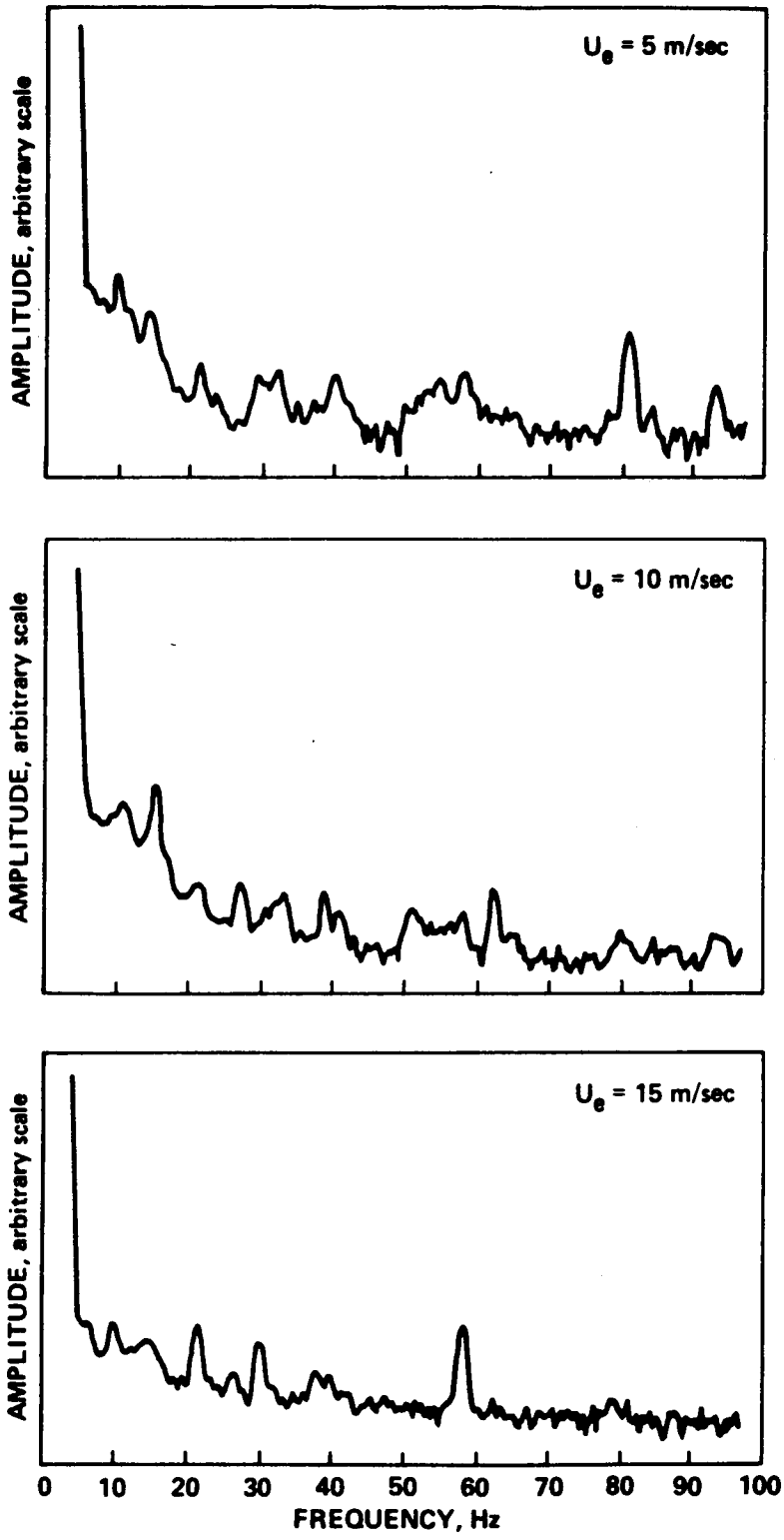

Figure 14. U-component Spectra Measurements, low-speed side.

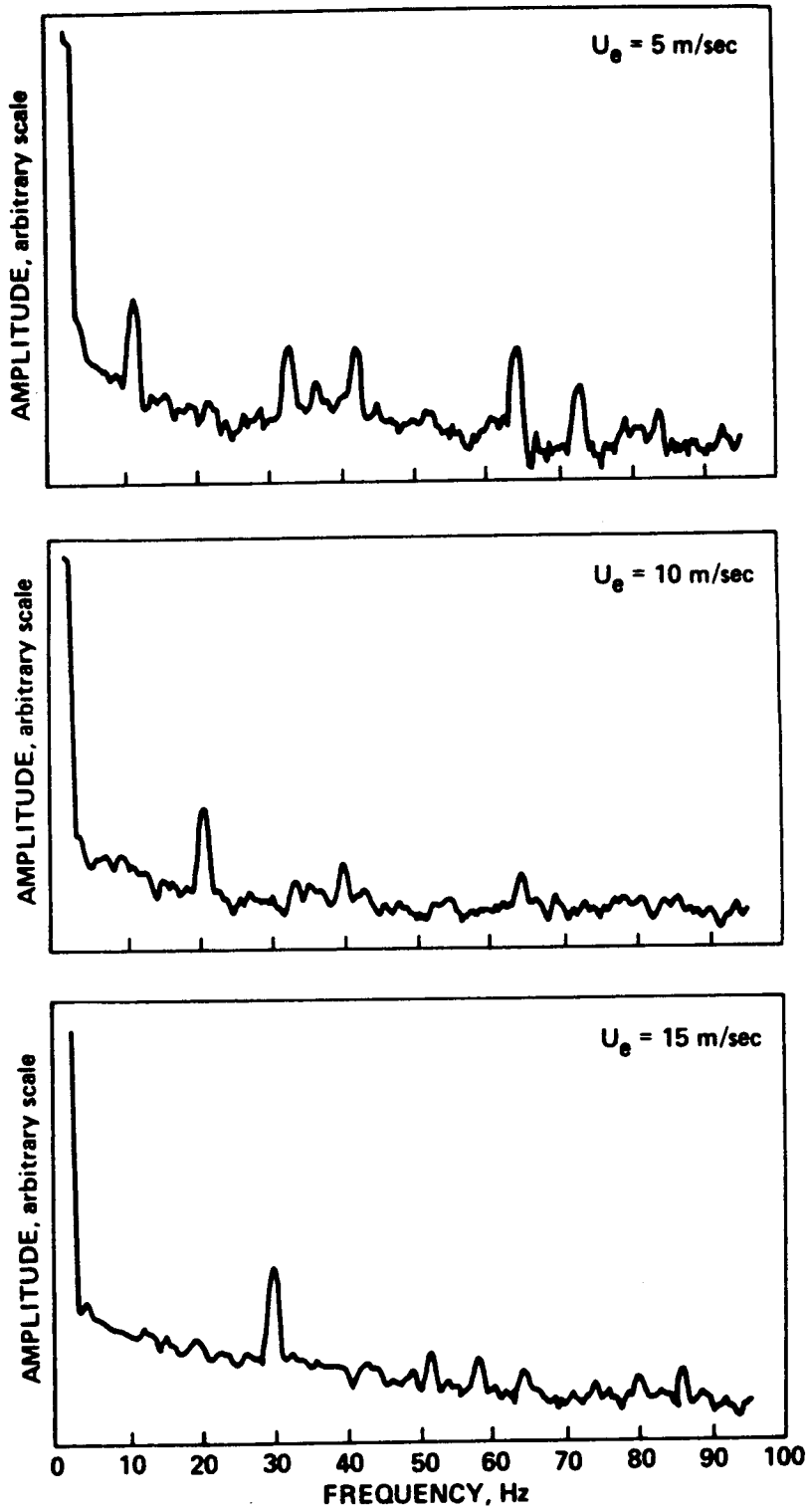

Figure 15. U-component Spectra Measurements, high-speed side.